

光学学报

主被动星载大气探测载荷性能对比与分析

王静松^{1,3}, 刘东^{1,2*}

¹中国科学院合肥物质科学研究院安徽光学精密机械研究所中国科学院大气光学重点实验室, 安徽 合肥 230031;

²先进激光技术安徽省实验室, 安徽 合肥 230037;

³中国科学技术大学研究生院科学岛分院, 安徽 合肥 230026

摘要 卫星遥感能够获取全球范围的大气环境参数, 主要包括主动和被动两类探测技术。星载激光雷达作为典型的主动光学遥感载荷可以用于探测全球大气气溶胶、云、大气风场和温室气体等, 并可以反演垂直廓线信息。本文概述了星载激光雷达探测技术的发展历程, 较为全面地总结了星载激光雷达载荷轨道及技术参数, 并与被动光学遥感载荷进行了比较, 探讨了主被动星载大气探测载荷各自的优劣势和未来发展趋势。通过对比分析, 为未来不同应用场景的大气探测载荷选择提供参考, 有助于更好地利用卫星数据反演全球大气参数。

关键词 星载激光雷达; 主被动遥感; 光学载荷; 大气环境参数; 大气探测

中图分类号 TN958.98 文献标志码 A

DOI: 10.3788/AOS231153

1 引言

大气环境参数直接影响地球的生态环境和气候变化, 从而影响人类的生命健康^[1], 例如气溶胶、云和温室气体等通过对太阳光发生吸收和散射作用影响太阳和地球之间的辐射平衡, 是造成大气环境污染和极端天气频发的重要原因^[2]。同时大气层作为航空航天作业区域, 大气温度、压强、密度和大气风场等环境参数对装备的设计和性能指标的实现有着举足轻重的影响^[3]。故全球大气环境参数探测一直以来备受各国学者关注。

卫星遥感是一种获取全球大气环境参数的重要技术手段, 可分为主动和被动探测两大类别。主动探测又称为有源探测, 自身带有辐射源, 向目标物发射不同形式的电磁波, 不依赖于太阳光, 可昼夜工作, 常见的主动遥感有激光雷达^[4-5]、合成孔径雷达^[6]、微波散射计^[7]等。被动探测即无源探测, 自身无辐射源, 需要借助目标物的反射或自然辐射源(如太阳)的电磁波, 基于该探测技术的遥感仪器有中分辨率成像光谱仪^[8]、测风干涉仪^[9]、云与气溶胶偏振成像仪等^[10]。相对于主动星载探测技术而言, 被动探测载荷发展历史悠久, 技术更加成熟, 遥感仪器种类和探测目标多样, 但存在如依赖于太阳光、探测时间及区域具有局限性等问题。以激光雷达为代表的主动星载探测技术弥补了这些缺点, 主被动星载遥感大气探测技术协同发展, 为全球大

气环境参数探测提供了有力的技术支撑。

目前卫星遥感大气环境探测在云、气溶胶、大气风场、温室气体、温度、压强和密度等参数的探测上作出了巨大贡献, 有效解决了大气污染、气候变化等问题。本文介绍了星载激光雷达的发展历程, 重点对比分析了主被动星载遥感载荷对主要的大气环境参数进行探测的优缺点, 最后总结探讨了主动星载激光雷达和被动遥感大气环境参数探测技术的未来发展趋势。

2 星载激光雷达探测大气环境参数

主动星载高精度探测大气环境参数的载荷主要为激光雷达, 自 1960 年第一台激光器的成功研制, 激光雷达从诞生到应用已经六十余年, 大气探测是激光雷达最先应用、也是最为成熟的领域。按照平台划分, 可以将大气探测激光雷达分为地基、空基和天基三种, 地基因其探测时间地点方便灵活、人工维护方便和安全性高风险小等优点使得它的探测种类全面且多样, 包括米散射激光雷达、偏振激光雷达、拉曼激光雷达、高光谱分辨率激光雷达、多普勒激光雷达、差分吸收激光雷达、共振荧光激光雷达和瑞利散射激光雷达等。激光雷达空基探测主要建立在机载方面, 相对于地基激光雷达优势较为明显, 解决了人迹罕至地区地基激光雷达无法设立站点的难题, 大大增加了探测的范围, 常作为星载激光雷达的验证手段。但上面两种探测方式都无法满足全球范围内的连续探测, 随着全球环境和

收稿日期: 2023-06-19; 修回日期: 2023-07-23; 录用日期: 2023-08-11; 网络首发日期: 2023-08-15

基金项目: 安徽省自然科学基金(2208085UQ01)、合肥研究院院长基金拔尖人才培育项目(BJPY2021A03)

通信作者: *dliu@aoifm.cas.cn

气候变化等研究的迫切需求,星载激光雷达在地基和机载的研究基础上逐渐发展壮大^[11-12]。

1994年9月,美国国家航空航天局(NASA)为了验证星载激光雷达探测的关键技术和发展卫星平台的应用,开展了激光雷达空间技术实验(LITE),一台三波长激光雷达搭载在“发现号”航天飞机上飞行了10天,LITE的设计能够获得云层、平流层和对流层中的气溶胶、大气边界层的高度以及25~40 km高度之间平流层的大气温度和密度。LITE首次获得了全球范围气溶胶垂直廓线数据,利用地基和机载激光雷达对其进行验证,LITE在南大西洋部分地区观测得到的气溶胶散射比与NASA P-3B机载飞行数据一致性较好^[13]。Osborn等^[14]获取了LITE的532 nm和355 nm高质量平流层气溶胶测量结果,得到了气溶胶垂直结构和光学特性的全球视图,该数据还可用于气溶胶空间分布和传输。Menzies等^[15]利用LITE的海面后向散射反演海面风速,表明了星载激光雷达反演大气风场的可行性,LITE虽然工作时间较短,但为星载激光雷达大气探测打下良好的基础,具有里程碑式的意义^[16-17]。欧洲航天局(ESA)于1991年正式启动欧洲第一个星载激光雷达计划——大气激光雷达(ATLID)开发计划^[18]。该激光雷达的二极管泵浦固体Nd:YAG激光器发射1064 nm波长的激光脉冲,后向散射光被直径为0.6 m的扫描望远镜所接收,期望获得云、对流层气溶胶和大气边界层等大气参数,原计划发射在极地轨道800 km高度,最后因为种种原因没有如期发射^[19-21],但为地球云-气溶胶和辐射探测卫星(EarthCARE)计划提供了宝贵的经验。EarthCARE计划是一项由ESA与日本宇宙航空研究开发机构(JAXA)联合进行的对地观测任务,将主动和被动遥感仪器组装在一起进行探测,卫星搭载四种载荷,分别为ATLID、多光谱成像仪(MSI)、宽带辐射计(BBR)和云剖面雷达(CPR),旨在提供光学薄云和气溶胶的垂直剖面图以及云边界的高度,加强人类对云-气溶胶-辐射相互作用和地球辐射平衡的理解,具有独特的多普勒功能并测量云粒子的垂直速度,另外其运行轨

道降至394 km,增加了云探测灵敏度^[22-24]。ATLID是一种高光谱分辨率激光雷达(HSRL),基于Fabry-Perot标准具将大气米散射和瑞利散射信号分离,选择紫外光谱范围内的工作波长355 nm,望远镜直径为620 mm。该计划一再推迟,预计2024年发射^[24]。

冰、云和陆地高程卫星(ICESat)主要搭载地球科学激光测高系统(GLAS)(图1),是全球首颗对地观测激光测高卫星^[25]。ICESat从2003年发射升空至2010年退役,期间提供了冰盖质量均衡、陆地地形、植被、云和气溶胶的分布和垂直结构等数据,为人类了解地球大气和气候变化如何影响极地冰和全球海平面提供了科学依据。GLAS设计有三个激光器,使用波长分别为1064 nm和532 nm的红外和可见光激光脉冲,分别主要对应地表与大气,以40 Hz的频率连续发射,后向散射光被直径为1 m的望远镜接收^[26-28]。Hlavka等^[29]在美国加利福尼亚州的一次火灾案例中,应用GLAS获取了气溶胶和云的光学厚度,与云物理激光雷达(CPL)一致性较好,Hart等^[30]研究发现,GLAS数据能够探测40 km高空大气中气溶胶层分布,ICESat/GLAS被证实其探测云和气溶胶的能力,展示了星载激光雷达在大气科学中的重要作用。作为ICESat的后续任务,美国NASA于2018年9月又发射了ICESat-2卫星,搭载高级地形激光高度计系统(ATLAS),与GLAS不同的是,首次引入的单光子探测技术大大提高了对地探测数据获取频率^[31]。ATLAS为单波长激光雷达系统,只有532 nm波长,配备的高重复频率激光器每秒对地发射1万次光脉冲,采用光子计数体制,优化了对地高程测量技术^[32]。虽然ICESat-2卫星主要目的是高分辨率测高,但是依然记录从14 km高度到地表的云层和气溶胶的后向散射信息,这为了解气候变化、冰盖消融和海平面上升之间的相互关系提供了科学依据,但14 km的低高度对于背景计算和校正带来困难,造成白天信号不理想,需要在算法上突破。另外,在云和气溶胶的识别中,由于ATLAS只有一个波长工作,缺乏偏振探测通道,无法识别大气中的非球形粒子^[33-34]。

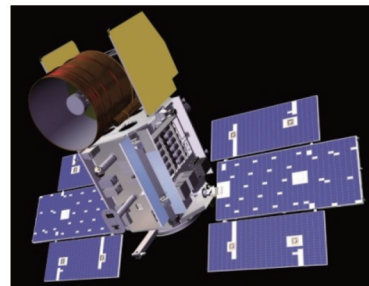


图1 ICESat(左)和GLAS(右)模型图^[25]

Fig. 1 ICESat (left) and GLAS (right) models^[25]

LITE和ICESat为后面大气探测激光雷达的研制提供了宝贵的经验,但他们搭载的激光雷达并没有测

量后向散射信号的偏振信息^[35]。美国NASA与法国国家太空研究中心(CNES)合作开发的云-气溶胶激

光雷达和红外探路者卫星观测(CALIPSO)搭载的正交偏振云-气溶胶激光雷达(CALIOP)是一种采用双波长具备偏振探测能力的激光雷达(图2),另外还有在可见光和红外光谱区域工作的被动成像仪、成像红外辐射计(IIR)和宽视场相机(WFC)^[36]。二极管泵浦Nd:YAG激光器运用调Q和倍频发射1064 nm和532 nm的线偏振光脉冲,重复频率为20.2 Hz,能量为110 mJ,望远镜直径为1 m^[37]。在低对流层,激光雷达空间分辨率表现为垂直方向上30 m,水平方向333 m。被动遥感仪器IIR幅宽64 km,提供8.65、10.60和12.05 μm的辐射测量,优化联合激光雷达探测卷云和粒子尺度,WFC为改进的星跟踪器相机,幅宽61 km,覆盖620~670 nm波长的光谱区域,为激光雷达测量提供气象背景^[38-39]。CALIOP为星载激光雷达技术取得突破性发展作出了重要贡献,截至目前已经在轨运行了17年,远远超过了预期设计,为气溶胶-云-降水的相互作用、全球沙尘分布、传输和污染、天气和气候变化研究等科学问题提供了科学数据^[4-5, 40]。CloudSat卫星和CALIPSO卫星共同组成A-Train卫星星座,CloudSat卫星是世界首颗专门用于观测全球云层特征的微波主动探测卫星,其上搭载的毫米波云廓线雷达(CPR)额定频率为94 GHz,采用天底观测方式,CPR可以探测垂直剖面125层,垂直分辨率为240 m,水平分辨率为1.4 km×2.5 km,CPR具有较强的穿透云层的能力。国内学者^[41]利用CloudSat卫星在2006—2009年的数据分析中国及周边地区的云垂直结构特征,并根据气候区域统计分析了云垂直结构分布特征。张华等^[42]利用CloudSat数据资料研究了东亚地区的

云垂直结构,首次计算了气候模式的云辐射过程中表征云的垂直结构特征的抗相关厚度参数,分析该参数的季节变化和空间分布,并讨论抗相关厚度对云辐射强迫计算的影响。杨冰韵等^[43]利用CloudSat数据产品对云微物理特征量(云中液态水/冰水含量和路径、云滴有效半径等)和云光学参数(云光学厚度等)的全球分布及季节变化进行了统计分析,为推动气候模式及参数检验的发展提供了有效方案。李积明等^[44]利用CALIPSO激光雷达数据研究了东亚地区云的垂直分布特征,重点分析了云垂直分布特征在各子区域的季节变化特征。研究表明,CPR具有穿透较厚云层的优势,CALIOP对于卷云、高积云等光学厚度较小的云层有着精细的探测,CloudSat和CALIPSO协同观测将有效提高云参数反演。Sassen等^[45]探测得到卷云的高度和厚度以及全球时空特征,卷云发生频率为16.7%。郑建宇等^[46-47]利用二级云产品数据分析了8种云类及三相态的云量地理分布、纬向垂直分布的季节变化特征以及云层分布概率,另外分析了3种不同类型的热带深对流云团的差异。Omar等^[48]介绍了CALIOP气溶胶分类算法和激光雷达比的选择方案,给出了气溶胶类型的全球分布。Oliveira等^[49]采用CALIOP、MODIS、AERONET和地基激光雷达对2005—2016年巴西东北部气溶胶光学特性进行分析,确定了气溶胶的类型。孙雨辰等^[50]利用CALIOP数据对6种气溶胶的全球分布和光学特性进行统计分析,利用其中的退偏比和色比值有效识别大气中的吸收性气溶胶沙尘。另外,中国海洋大学利用CALIOP进行了大量海洋风场的反演工作^[51-53]。

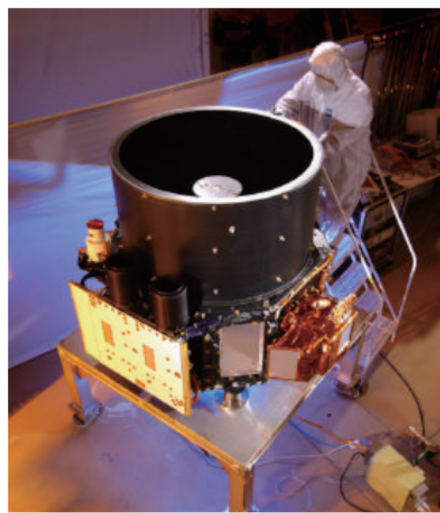


图2 CALIOP有效载荷(左)与其功能框图(右)^[39]
Fig. 2 CALIOP payload (left) and its functional block diagram (right)^[39]

美国NASA为了衔接上CALIPSO和EarthCARE的数据,于2015年1月将云气溶胶传输系统(CATS)安装在国际空间站(ISS)的日本希望号实验舱——“暴露设施”(JEM-EF)上。CATS也是迄

今为止唯一搭载在空间站上的激光雷达系统,拥有两个高重复频率低能量的Nd:YVO₄激光器,采用光子计数方法获得云和气溶胶的垂直分布特性,在33个月的在轨运行中,发射了超过2000亿个激光脉冲,基于这

些设计参数和运行平台,它具有直接校准1064 nm信号的独特之处^[54-55]。CATS有三种工作模式(图3),分别为多波束模式、HSRL模式和紫外模式:多光束模式将来自第一个激光器的能量分为1064 nm和532 nm两个波长,用于探测云和气溶胶的属性,但由于激光电子设备的故障,该模式不能继续使用;HSRL模式使用第二个激光器,采用了HSRL技术,目的是提供更加精确的气溶胶消光系数测量,但该激光器的频率稳定性问题限制了数据的质量;紫外模式同样也使用第二个激光器,在1064 nm和532 nm波长的基础上增加了355 nm波长,为探索355 nm波长在天基激光雷达上的应用积累经验,由于激光光路的故障,CAST在该模式

下不能正常工作。CATS首次开机后飞越非洲地区,获得了撒哈拉沙尘高达5 km、卷云延伸超过17 km,以及南非生物质燃烧产生的烟雾的相关结果,与CALIPSO的结果对比一致性较好^[56]。CATS在国际空间站上从2015年2月10日运行至2017年10月30日,提供了1064 nm和532 nm大气垂直后向散射廓线,得到了1064 nm波长比以往星载激光雷达更高的信噪比,可直接进行大气校准,对于气溶胶光学厚度,CATS与AERONET、MODIS和CALIOP等星载被动遥感仪器具有合理的一致性,可利用CATS数据获取全球气溶胶日变化特征^[57-58]。

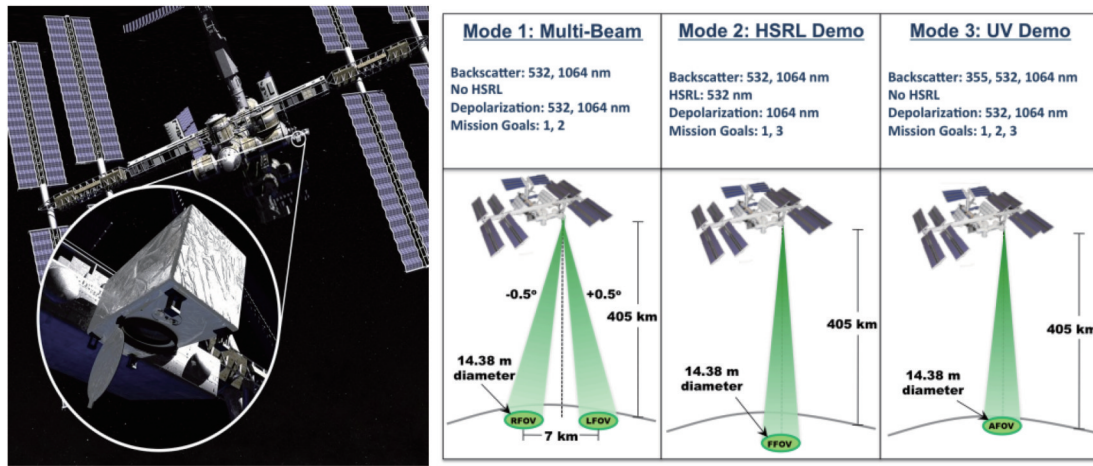


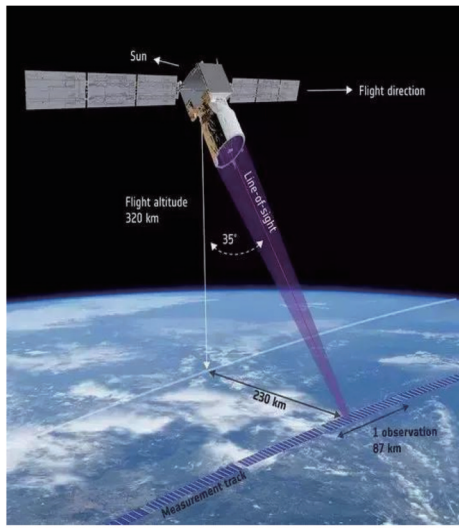
图3 CATS在国际空间站(左)^[54]上的三种工作模式(右)^[56]

Fig. 3 CATS on ISS (left)^[54] in three working modes (right)^[56]

为了获取全球大气三维风场信息,ESA于2018年8月22日成功发射了风神(ADM-Aeolus)卫星(图4),其上搭载了大气激光多普勒仪器(ALADIN),是首个获取全球大气风场的多普勒测风激光雷达^[59]。星载多普勒测风激光雷达技术可分为相干测风、直接测风和混合体制测风技术,星载多普勒相干测风激光雷达因为研制难度较大,一直未实践^[60]。1987年,NASA计划在对地观测系统卫星EOS上搭载激光大气测风仪(LAWS)系统,开创了星载多普勒测风激光雷达的先河,但最终因为预算等原因终止了计划^[61]。1998年,NASA再次提出了空间准备相干激光雷达实验(SPARCLE)计划,以及日本邮政省通信研究实验室与美国相干技术公司(CTI)联合准备在国际空间站上搭载多普勒相干测风激光雷达系统(JEM/CDL)等^[62-63]。星载多普勒混合体制激光雷达如NASA在2006年提出的混合多普勒风力激光雷达(HDWL)采用2051 nm和355 nm激光进行全球大气风场探测^[64]。相对于其他两种体制测风激光雷达,ALADIN采用较为成熟的直接测风激光雷达技术,根据多普勒效应,通过输出脉冲与后向散射信号之间的延迟就能获取大气中不同高度的风速、方向和移动距离等参数。

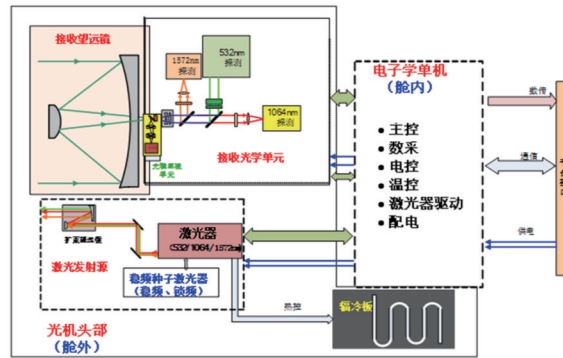
ALADIN由三大部分组成:激光发射器(工作波长为355 nm)、米散射及瑞利后向散射信号接收器组件和直径为1.5 m的卡塞格林望远镜。ALADIN拥有3个通道,其中2个通道采用法布里-珀罗干涉仪(FPI)鉴频技术接收处理大气分子信号,1个通道采用斐索干涉仪分析气溶胶和云的后向散射信号^[65-66]。ADM-Aeolus的任务要求为获取20 km左右以下的全球风廓线,对于地表以上2~16 km和16~20 km范围内分别实现2~3 m/s和3~5 m/s的测量精度,每50 km足迹内获得一次平均风速,每小时风廓线数达120条^[59]。ALADIN作为目前唯一在轨的星载大气风场探测激光雷达已经运行了4.5年,在2023年4月30日停止工作,但ADM-Aeolus展示了星载激光雷达高精度、强实时性的测风能力,为提高天气与气候预报的准确性、改善大气模式和推进大气动力学研究作出了巨大贡献。

国内星载激光雷达起步较晚。2022年4月16日,我国将气溶胶-云探测激光雷达(ACDL)(图5)、紫外高光谱大气成分探测仪(EMI)、多角度偏振成像仪(DPC)、高精度偏振扫描仪(POSP)和宽幅成像光谱仪(WSI)搭载在大气环境监测卫星(DQ-1)上发射升空(图5)。ACDL同时发射532、1064、1572 nm三波长

图4 ADM-Aeolus探测系统原理^[59]Fig. 4 ADM-Aeolus detection system schematic^[59]

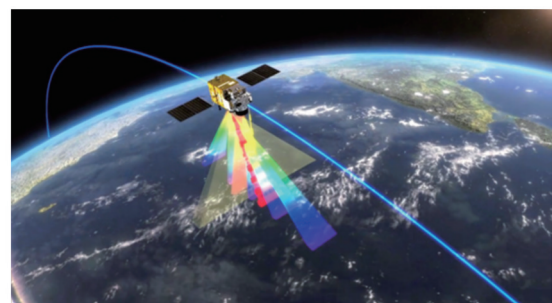
双脉冲激光,基于路径积分激光差分吸收(IPDA)和HSRL技术全天时、高精度地获取全球云、气溶胶垂直廓线分布和CO₂柱线浓度等大气环境参数,也是国际

上目前唯一在轨运行的主动探测温室气体星载激光雷达^[67]。ACDL拥有5个接收通道,分别是532 nm气溶胶高光谱通道、532 nm气溶胶混合平行通道、532 nm气溶胶混合垂直通道、1064 nm气溶胶探测通道和1572 nm二氧化碳探测通道。1572 nm波长重复频率为20 Hz,532 nm和1064 nm波长的重复频率为40 Hz,望远镜口径为1 m,预期CO₂柱线浓度测量精度为 1×10^{-6} ,气溶胶光学参数为15%的不确定度。ACDL是目前国际上输出波长最多、输出能量最高、激光稳定性最高的星载激光雷达,首次采用IPDA技术获取全球CO₂柱线浓度,也是首次基于碘分子滤波器的HSRL技术探测气溶胶和云的光学参数。EMI具有2600 km的观测幅宽,通过对污染气体光谱信息的识别可获取单日全球的NO₂、SO₂和O₃浓度信息,DPC和POSP在国际上首次运用“偏振交火”的载荷方案实现对气溶胶光学厚度和粒径分布等的观测。DQ-1卫星结合5台主被动遥感仪器协同探测,实现了大气环境要素同步测量,在全球气候变化和空气质量监测方面作出了巨大贡献^[68-69]。

图5 DQ-1(左)和ACDL系统功能图(右)^[69]Fig. 5 DQ-1(left) and ACDL system functional diagram (right)^[69]

2022年8月4日,我国首颗森林碳汇主被动联合观测卫星“句芒号”(CM-1)在太原发射升空,运行在506 km的太阳同步轨道上(图6),轨道倾角为97.4°,覆盖周期为59 d,标志着我国碳汇监测进入遥感时代^[70]。陆地生态系统碳监测卫星搭载了多波束激光雷达(CASAL)、多角度偏振成像仪(DPC)、多角度多光谱相机(DMC)和超光谱探测仪(FSI)等多台载荷,以主被动结合的探测方式获取陆地生态系统植被生物量、大气气溶胶和植被叶绿素荧光等信息,为我国在森林冠层高度监测、叶绿素荧光分布和大气环境与气候监测方面提供广泛的应用价值。其中CASAL部分分为植被子系统和气溶胶子系统,分别配置5个1064 nm波长和1个1064 nm/532 nm双波长的激光波束,5个40 Hz的激光波束监测森林冠层高度和结构,以及有效探测云和气溶胶的垂直结构^[71-73]。

美国NASA的气溶胶-云-生态系统(ACE)任务在

图6 CM-1在轨运行^[70]Fig. 6 CM-1 operating in orbit^[70]

21世纪初被提出,旨在量化气溶胶与云的相互作用,缩小气溶胶-云-降水相互作用的不确定性,评估气溶胶对水文循环的影响,确定海洋碳循环和其他海洋生物过程。载荷激光雷达部分采用三波长(355、532、1064 nm)HSRL技术,另外还包括多光谱偏振成像仪

(MSPI)、用于海洋遥感仪器的水色多通道光谱仪(ORCA)以及双频云雷达(CPR)等^[74-76]。

星载全球温室气体主动探测在ACDL成功发射之前,美国、日本等国家以及欧洲的一些国家开展了一系列基于IPDA技术的星载激光雷达任务和机载验证试验。2007年,美国NASA提出了夜间、白天和季节性CO₂排放主动监测计划(ASCENDS),该计划将测量全球大气中CO₂的浓度,包括陆地和海洋的CO₂的源和汇,且不分季节、纬度、白天和黑夜,以及气压和温度的变化。在计划提出后,美国戈达德航天中心(GSFC)、兰利研究中心(LRC)等多家单位进行了大量的验证分析实验,证明其可行性^[7-80]。运行轨道在450 km,望远镜直径为1.5 m,采用HgCdTe雪崩二极管(APD)探测器。该卫星原计划于2025年发射升空,具体计划目前冻结中,设计寿命达3年^[81]。

2008年,ESA提出了地球先进空间碳和气候观测任务(A-SCOPE),以更好地量化全球碳循环,弥补地基组网观测缺陷,发展星载激光雷达技术,在1000 km×1000 km的尺度上,小于0.02 Pg C yr⁻¹的不确定度范围内确定全球CO₂的源和汇。A-SCOPE星载计划同样基于IPDA技术,确定了两种探测波段,分别为1.57 μm(on-line位于6361.2246 cm⁻¹,off-line位于6356.50 cm⁻¹)和2.05 μm(on-line位于4875.6487 cm⁻¹,off-line位于4875.22 cm⁻¹),通过选择合适的CO₂吸收谱线,优化CO₂差分吸收值,减小温度的灵敏度和水汽的干扰,对于这两种不同波段选择,配置不同的激光雷达硬件参数,该计划在2014年暂时

取消^[82-84]。

2017年,法国航天局(CNES)联合德国航天局(DLR)共同研制大气甲烷遥感激光雷达任务(MERLIN),该激光雷达是唯一搭载的科学仪器,由DLR负责提供,旨在提供覆盖全球的甲烷气体循环信息,完善现有的温室气体监测系统^[85]。MERLIN采用1645 nm波段IPDA方法(图7),吸收峰波长在1645.552 nm处,吸收谷波长在1645.828 nm处,获取高精度XCH₄,目标随机误差优于27×10⁻⁹,系统误差优于3.7×10⁻⁹^[86]。MERLIN运行在500 km高度的轨道上,单脉冲能量为9 mJ,重复频率为20 Hz,设计寿命为3年,卫星发射时间预计在2026年后^[87]。

国际上主要的星载激光雷达载荷及其主要技术参数分别如表1和表2所示。

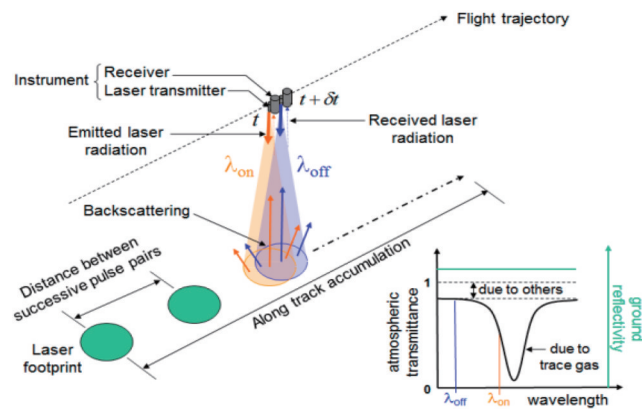


图7 IPDA方法原理图^[86]

Fig. 7 Schematic diagram of IPDA method^[86]

表1 国际上主要的星载激光雷达载荷
Table 1 Main international spaceborne Lidar payload

Platform Lidar payload	SSD LITE	CALIPSO CALIOP	ICESat GLAS	ICESat-2 ATLAS	ISS CATS	Aeolus ALADIN	DQ-1 ACDL	CM-1 CASAL
Total satellite weight /kg	—	587	970	1514	—	1400	2600	2936
Launch year	1994	2006	2003	2018	2015	2018	2022	2022
Type of orbit	Non-solar synchronous	Solar synchronous	Non-solar synchronous	Non-solar synchronous	Non-solar synchronous	Solar synchronous	Solar synchronous	Solar synchronous
Orbital altitude /km	260	705	600	500	405	320	705	506
Orbital inclination /(°)	57	98.2	94	92	51.64	97	98.135	97.421
Repetition period /d	—	16	91	91	3	7	51	59
Design life	10 d	3 a	3 a	3 a	0.5 a	3 a	3 a	8 a
Target of detection	Clouds, aerosols, etc.	Clouds, aerosols, etc.	terrain, clouds, aerosols, etc.	Ice, terrain, vegetation, etc.	Clouds, aerosols, etc.	Wind fields, clouds, aerosols, etc.	CO ₂ , clouds, aerosols, etc.	Vegetation biomass, chlorophyll fluorescence, aerosol, etc.

表2 国际星载激光雷达主要技术参数
Table 2 Main technical parameters of international spaceborne Lidars

Payload	Spatial resolution				Transmitting unit				Receiving unit			
	Vertical	Level	Laser	Wavelength	Single pulse energy	Repeat frequency	Pulse width	Divergence angle	Telescope diameter	Field of view	Photovoltaic conversion	
LITE	35 m	740 m	Nd: YAG	355, 532, and 1064 nm	500 mJ @532 nm	10 Hz	—	1 mrad	1 m	—	PMT@ 355 nm, APD@ 532 nm 1064 nm	
					500 mJ @1064 nm							
					160 mJ@ 355 nm							
CALIOP	30 m	333 m	Nd: YAG	532 and 1064 nm	110 mJ@ 532 nm	20.16 Hz	20 ns	0.1 mrad	1 m	0.13 mrad	PMT @532 nm APD@ 1064 nm	
					110 mJ@ 1064 nm							
					110 mJ@ 355 nm							
GLAS	Course 170 m Lateral (maximum) 15000 m Lateral (minimum) 2500 m	Nd: YAG	532 and 1064 nm	1064 nm 35 mJ@ 532 nm	75 mJ@ 1064 nm	40 Hz	5 ns	0.11 mrad	1 m	0.475 mrad@ 1064 nm 0.15 mrad @ 532 nm	SiAPD	
					532 nm							
					532 nm							
ATLAS	Course 90 m Lateral (two strong or two weak) 3300 m Lateral (strong and weak) 2500 m	Nd: YVO ₄	532 nm	0.12 mJ Weak: 0.04 mJ	Strong:	10 KHz	1 ns	0.024 mrad	0.8 m	83 μrad	PMT	
					Weak:							
					0.04 mJ							
CATS	25 m	15 m	Nd: YVO ₄	355, 532, and 1064 nm	2 mJ	4 kHz	30 ns	0.03 mrad	0.6 m	110 mrad@ +/ -0.5°	PMT @355 nm, 532 nm APD@ 1064 nm	
ALADIN	0.25– 2.00 km	87 km	Nd: YAG	355 nm	150 mJ	100 Hz	15 ns	12 μrad	1.5 m	22 μrad	CCD	
ACDL	30 m	337.5 m	Nd: YAG	532, 1064, and 1572 nm	mJ@532 nm ≥110 mJ@ 1064 nm ≥75 mJ@ 1572 nm	20 Hz@ 1572 nm	ns@ 1064 nm	≤50 nm	100 μrad	1 m	0.2 mrad	PMT @532 nm APD@ 1572 nm APD@ 1064 nm

续表

Payload	Spatial resolution				Transmitting unit					Receiving unit		
	Vertical	Level	Laser	Wavelength	Single pulse energy	Repeat frequency	Pulse width	Divergence angle	Telescope diameter	Field of view	Photovoltaic conversion	
CASAL	≤ 30 m	—	—	532 and 1064 nm	73 mJ@ 1064 nm 110 mJ@ 1064/ 532 nm	40 Hz	—	$40\text{--}60 \mu\text{rad}$ @1064 nm $\leq 200 \mu\text{rad}$ @1064/ 532 nm	1 m	—	APD	
ACE	—	—	Nd: YAG	355, 532, and 1064 nm	—	—	—	—	1.5 m	—	PMT @355 nm, 532 nm APD@ 1064 nm	
ATLID	40 m	—	Nd: YAG	1064 nm	100 mJ	100 Hz	20 ns	125 μrad	0.6 m	—	APD@ 1064 nm	
EarthCARE	500 m@ 20-40 km	282 m	Nd: YAG	355 nm	38 mJ	51 Hz	25 ns	45 μrad	0.62 m	75 μrad	PMT @355 nm	
MERLIN	—	—	Nd: YAG	1645 nm	9 mJ	20 Hz	20– 30 ns	—	0.69 m	—	APD @1645 nm	
A-SCOPE	—	—	Nd: YAG Ho- Tm: YAG	1.57/ 2.05 μm	50/55 mJ	50 Hz	—	0.435/ 0.2 mrad	1 m	0.476/ 0.22 mrad	APD	
ASCENDS	—	—	—	1572 nm	—	10 kHz	—	—	1.5 m	—	APD	

3 被动星载遥感探测大气环境参数

3.1 被动星载遥感探测云

1960年,美国发射了第一颗气象卫星TIROS-1,开启了卫星云遥感观测的新纪元^[88],随后日本、俄罗斯、中国等国家和欧洲的一些国家相继发射众多被动卫星,我国具有代表性的是风云气象卫星^[89-90]。风云三号G星于2023年4月16日发射升空,截至目前我国共发射了20颗风云气象卫星,实现极轨卫星和静止卫星的业务化运行。我国新一代极轨气象卫星风云3号D星(FY-3D)于2017年11月15日发射升空,运行在近极地太阳同步轨道上,与FY-3C形成组网观测。FY-3D搭载了10台先进的遥感仪器,包括中分辨率光谱成像仪(MERSI-II)、微波成像仪(MWRI-II)、红外高光谱大气探测仪(HIRAS-I)等,MERSI-II总通道数25个,其中250 m地面分辨率通道6个,其余为1000 m,从而可以获取全球250 m分辨率红外分裂窗区观测资料,红外探测能力较I型大幅提高,光谱覆盖范围为0.47~12 μm ,增加了1.38 μm 短波红外卷云探

测通道。MERSI-II云顶参数的反演一般采用其中的2个红外分裂窗通道亮温算法,张森等^[91]采用精度更高的一维变分法反演FY-3D/MERSI-II云顶温度、高度和压强参数,再利用AQUA/MODIS的云产品数据对FY-3D/MERSI-II的水云和厚冰云云顶参数进行精度检验,其中水云云顶高度精度为1.4 km±1.8 km。

我国风云四号A星(FY-4A)于2016年12月发射,标志着我国新一代静止气象卫星的新时代到来,使我国首次获得彩色卫星云图^[92]。FY-4A上搭载着先进的静止轨道辐射成像仪(AGRI)、干涉式大气垂直探测仪(GIIRS)、闪电成像仪(LMI)和空间环境监测仪(SEP)。AGRI主要承担获取云图的任务,空间分辨率表现为可见和近红外波段为0.5~1 km,红外波段为2~4 km,拥有14个通道,中心波长范围为0.47~13.5 μm ,在观测云的基础上区分云的不同相态,其原理是根据冰云和水云在短波红外1.6 μm 和2.2 μm 处吸收性不同的特性来区分^[93]。云的光学厚度和云有效半径影响着云在可见光波段和近红外波段的反射率,

故可利用AGRI的不同通道进行云参数反演。袁锦涵等^[94]基于FY-4A/AGRI的一级产品反演了云光学厚度和有效粒子半径,并研究了不同云滴谱对云光学厚度和有效粒子半径的影响,与MODIS反演结果相比一致性较好。

我国高分5号卫星(GF-5)搭载的多角度偏振相机(DPC)主要用于获取云和气溶胶的微物理信息,由中国科学院安徽光学精密机械研究所研制。它的设计借鉴了法国的POLDER/PARASOL,空间分辨率由6.2 km提高至3.3 km,水云和冰云在热红外波段处吸收有差异,粒子形状不同,导致水云和冰云的偏振特性呈现差异,利用多光谱、多角度偏振特点获取全球气溶胶和云的时空分布信息^[95-96]。常钰阳等^[97]开发了一套云检测、云相态识别和云光学厚度的反演算法,将其应用到POLDER/PARASOL。Li等^[98]提出新的云检测方法,通过统计不同时间和地区的不同大气模型和下垫面获得新的动态阈值,从而提高了云识别的准确性,尤其是对于特殊地表类型,在此基础上开展了云相态和云光学厚度反演。

美国NASA研制的中分辨率成像光谱仪(MODIS)搭载在Terra和Aqua卫星上发射升空^[99]。MODIS每1~2天获取一次全球数据,拥有36个光谱波段,光谱范围从可见光0.405 μm覆盖到热红外14.385 μm,不同波段的分辨率范围从250 m到1000 m,提高了人类对陆地、海洋和低层大气中的全球动态过程的理解。MODIS被广泛应用到云遥感中,MODIS可以根据可见光和近红外的反射率、红外亮温差和反射率构造的指数和量温差等数据来进行云检测,云识别常用8.5 μm和11 μm热红外通道的亮温差进行云相态识别,该方法又称为双光谱法^[90, 100]。CO₂切片技术常用于MODIS反演云顶参数过程中,当波长范围从13.5 μm到15 μm变化时,CO₂对红外光的吸收能力不断增强,从而导致该波段内的信号受到不同影响,呈现差异^[90, 101-102]。Platnick等^[103]概述了CLDPROP_MODIS和CLDPROP_VIIRS云光学特性数据集算法和传感器件连续性的评估,包括云热力学相位、光学厚度和有效粒径等。

日本气象厅于2014年10月和2016年11月相继发射了Himawari-8和Himawari-9两颗静止轨道气象卫星,上面均搭载了先进葵花探测仪(AHI)。其中Himawari-8的AHI拥有16个波段,中心波长覆盖0.47~13.3 μm,空间分辨率为0.5~2 km。Iwabuchi等^[104]利用热红外波段测量数据提取云的宏观、微物理和光学特性,Himawari-8能够捕捉大气中云系统的连续时间的变化,证明了其频繁观测对云系统生命周期研究的实用性。

3.2 被动星载遥感探测气溶胶

气溶胶的星载被动遥感种类繁多,可以大致分为以下几类:多光谱遥感仪器、偏振遥感仪器和多角度遥

感仪器^[105-106]。多光谱遥感仪器是根据气溶胶对紫外至短波红外多光谱的吸收散射特性进行反演的,常见的星载多光谱遥感仪器包括甚高分辨率辐射仪(AVHRR)、中分辨率成像光谱仪(MODIS)和云与气溶胶成像仪(CAI)。AVHRR搭载在美国TIROS-N卫星、NOAA系列卫星和Metop系列卫星上,AVHRR-3拥有6个光谱通道,早期的AVHRR采用单通道反射比法探测海洋气溶胶的特性^[107]。赵柏林等^[108]利用NOAA-7搭载的AVHRR的可见光通道,光谱范围为0.58~0.68 μm,得到了晴天渤海海上空大气气溶胶光学厚度。随后将双通道算法应用到海上气溶胶反演中。Mishchenko等^[109]基于AVHRR数据发现双通道算法可以提供更准确、偏差更小的气溶胶光学厚度的反演,云筛选和校准是造成反演的误差来源。Hauser等^[110]利用NOAA-7的AVHRR数据反演得到中欧地区上空20个月的光学厚度,并使用11个AERONET站点进行评估,但不能用于亮地表区域,因为气溶胶信号灵敏度太低。国内学者^[111]利用背景合成算法对中国部分陆地区域进行气溶胶光学深度(AOD)的反演,并与MODIS进行对比。

MODIS有7个通道专门用于气溶胶光学特性研究,MODIS提供3种气溶胶光学厚度反演,分别为暗目标(DT)算法、深蓝(DB)算法以及暗目标和深蓝结合(DTB)算法,DT算法根据浓密植被和暗色土壤在红蓝波段反射率低,气溶胶信息相对敏感的特点进行反演,适用于植被表面;DB算法是基于历史数据,采用最小反射率方法构建地表反射率数据库进行AOD反演,适用于陆地AOD反演;DTB算法根据归一化植被指数结合DT与DB算法进行AOD反演^[105, 112]。毛节泰等^[113]利用MODIS数据反演陆地气溶胶再与北京大学地面多波段太阳光度计观测对比,研究发现二者相关性较好。Wei等^[114]利用更新后的DT算法对全球的MODIS C6.1版本产品进行验证,研究表明,该版本数据集在不同时空尺度上得到了全面改善。苏玥宇等^[115]也利用C6.1版本AOD产品进行验证,对比分析了不同气溶胶类型区域条件下3种算法的精度及误差,更好地了解了MODIS的AOD算法在中国不同类型区域的适用性。

多角度成像分光计(MISR)和MODIS一同搭载在美国Terra卫星上,具备4个可见光或近红外光谱波段及9个角度(±70.5°、±60.0°、±45.6°、±26.1°和0°)的多角度多光谱测量,空间分辨率为275 m~1.1 km^[116-117]。Kahn等^[118]利用MISR早期AOD算法在陆地和海洋上的性能进行定量评估,与全球分布的AERONET太阳光度计的两年测量记录进行比较,相比其他遥感仪器而言,MISR反演效果已经很好了。MISR除了反演AOD之外,还能分析全球气溶胶类型,为全球气候强迫和气溶胶传输等方面提供参考价值,与MODIS相比一致性很好,海洋上的AOD反演,

二者相关系数约为0.9^[119]。张艳婷等^[120]联合对比MODIS和MISR数据资料,得到了亚太经济合作组织(APEC)会议前期、期间、后期的AOD和Angstrom指数等气溶胶参数的时空分布特征。

中国科学院安徽光学精密机械研究所自主研制的多角度偏振成像仪(DPC)具有多光谱、多角度和偏振特点,DPC在法国的POLDER上做了很大的改进,性能得到了提高。2013年POLDER结束了探测任务,DPC成为主要的多角度偏振气溶胶探测遥感仪器^[95]。高分5号搭载的DPC光谱通道范围为443~920 nm,拥有8个波段,其中3个为偏振波段(490、670、865 nm),5个波段主要用于气溶胶反演(490、670、865、443、565 nm),沿轨最多可获得12个观测角度^[121-122]。在利用星载偏振遥感探测气溶胶时,传感器所接收到的信息包括地表和大气的总和,但地表的偏振信息影响DPC反演气溶胶,故地气解耦合尤为重要,提汝芳等^[123]基于GF-5的DPC近红外波段865 nm的数据,获取地表多角度偏振反射率数据,针对8种典型地表类型,对比分析了不同模型的双向偏振反射分布函数(BPDF)性能,为估算地表偏振反射率、更好地反演气溶胶参数提供了支持。Li等^[124]在一次严重雾霾污染天气中,首次用GF-5/DPC反演气溶胶成分含量和光学辐射性质,通过灵敏度评估了DPC反演的可行性、稳定性和不确定性,该研究使我国在多角度偏振卫星遥感探测方面处于国际先进水平。

3.3 被动星载遥感探测温室气体

被动星载遥感温室气体的原理是基于温室气体在特定波段的吸收特性,根据传感器接收的光谱信息进行定量反演,截至目前世界各国发射可用于探测温室气体的卫星达20多个^[125-126]。日本于1996年8月发射了首个可用于温室气体探测的先进地球观测卫星ADEOS,其上搭载的温室气体干涉监测仪(IMG)虽然只工作了8个月,但提供了第一张全球温室气体图,CO₂和CH₄的精度分别为2%和10%^[127]。2009年1月日本发射了全球首颗专用于温室气体探测的GOSAT卫星,该卫星配备了两个传感器,碳观测傅里叶变换光谱仪(TANSO-FTS)和云和气溶胶成像仪(TANSO-CAI),TANSO-FTS是基于Michelson干涉光谱技术,探测精度设计技术指标分别为 4×10^{-6} (CO₂)和 34×10^{-9} (CH₄)。2018年10月日本又发射了GOSAT-2,为GOSAT后继任务,探测精度有很大的提高,CO₂的探测精度设计技术指标为 0.5×10^{-6} ,CH₄为 5×10^{-9} ,并且将CO和PM_{2.5}纳入了探测范围^[128]。

欧洲在2002年3月发射了对地环境观测卫星Envisat-1,搭载大气制图扫描成像吸收光谱仪(SCIAMACHY),探测波段从紫外(约214 nm)到短波红外(约2386 nm),观测模式有天底、临边和掩星三种,SCIAMACHY通过8个通道获取多种温室气体的信息,CO₂和CH₄探测精度分别为3%和10%。Noel

等^[129]利用SCIAMACHY掩星测量得到的平流层CH₄和CO₂剖面。Frankenberg等^[130]获得了2003—2009年全球XCH₄的趋势。

美国NASA于2014年成功发射了碳观测者2号(OCO-2),同年加入了A-Train编队,该任务将揭示CO₂在大气中分布的过程,量化CO₂的源和汇。OCO-2搭载的光栅光谱仪有3个通道(1.61 μm的CO₂弱吸收波段、2.06 μm的强吸收波段和0.764 μm的O₂-A吸收带)^[131],利用地面TCCON站点进行对比验证,OCO-2反演结果一致性较好,绝对中值差小于 0.4×10^{-6} ^[132]。2019年5月,美国NASA发射了OCO-3至国际空间站上,与OCO-2进行协同观测,由于搭载平台差异及OCO-3使用了新的指向镜组件(PMA),引入了新的观测模式,即快照模式,改变了观测数据特征。其科学目标为获得全球高精度的XCO₂和太阳诱导荧光(SIF),提升对全球碳源和碳汇的监测水平^[133]。

我国的温室气体探测卫星发展较晚,2016年12月发射了TANSAT碳卫星,成为拥有国际上第三颗具备高精度探测温室气体能力的卫星的国家。TANSAT碳卫星搭载的高分辨率高光谱温室气体探测仪(ACGS)可以获取全球CO₂的浓度,探测原理与OCO系列卫星一致,空间分辨率为1.0 km×2.0 km。TANSAT的结果与TCCON站点、GOSAT和OCO-2对比验证后表现出高精度的探测能力^[134-135]。2018年5月高分5号卫星成功发射,高分5号卫星是世界首颗实现对大气和陆地综合观测的全谱段高光谱卫星,其中搭载的温室气体监测仪(GMI)由中国科学院安徽光学精密机械研究所自主研制,首次采用空间外差光谱技术(SHS)获取全球温室气体柱浓度,空间外差光谱技术结合了GOSAT的傅里叶变换光谱仪(FTS)技术和OCO-2的光栅光谱技术,具有极高的光谱分辨率^[136]。李勤勤等^[137]研究发现,气溶胶类型、地表反射率和地表气压等因素均影响GMI反演CO₂浓度,并利用TCCON站点对GMI反演结果进行验证,反演精度在1%以内。

3.4 被动星载遥感探测大气风场

被动星载遥感大气风场主要以云、水汽和大气成分等为探测目标进行反演,根据探测的原理可以将其分成两类:一是针对云和水汽目标成像,测量目标物在图像中的位移进行风场反演;二是根据大气成分的多普勒频移计算风速,这两类方法分别采用卫星天底观测模式和临边观测模式进行探测^[138]。2002年自旋增强可见光与红外成像仪(SEVIRI)搭载在欧洲第二代气象卫星(MSG)上发射升空,SEVIRI通过跟踪云和水汽特征获取大气风场,拥有12个通道,包括11个窄带宽和1个高分辨率宽带通道,具有较高的空间分辨率(4~6 km)^[139]。Nerushev等^[140]利用SEVIRI探测大气资料对水平风速矢量的计算进度进行了估计,并将结果与独立观测的数据和理论模型进行比较,结果几

乎一致。

基于干涉理论的被动星载探测大气风场的技术主要有Michelson干涉仪测风技术、Fabry-Perot干涉测风技术和多普勒差分干涉仪。干涉仪作为大气风场探测的核心部件,通过接收大气中具有一定多普勒效应的气辉发射线或大气吸收线,将信号转为干涉条纹的变化来反演风场等大气参数^[138, 141]。1991年9月由法国和加拿大联合研制的WINDII风成像干涉仪搭载在UARS卫星发射升空,成为全球首个采用Michelson干涉技术的星载被动大气风场遥感仪器,它在视场展宽、步进方式和相位热稳定控制测量风速等方面作出创新,成功探测到80~300 km高度范围的风速、温度和气辉体发射率等。WINDII有两个视场,分别与航天器速度成45°和135°角,因此可以从两个方向观察相同体积的大气,以确定风矢量^[142]。WINDII理论设计测风精度为10 m/s,但实际精度可达5 m/s,应用效果显著^[143]。

以高分辨率多普勒曾成像仪(HRDI)为代表的星载Fabry-Perot干涉测风技术成功获取了大气风场数据,于1991年搭载在上层大气研究卫星UARS上发射升空。HRDI采用三标准具串联,分辨率为0.05 cm⁻¹,具有很好的白天背景光抑制能力,目标是测量白天平流层(10~40 km)、中间层和低热层(65~110 km)以及夜间中间层(约95 km)的矢量风,探测精度达到5 m/s^[144],水平风矢量是通过测量沿两条视线的分子氧旋转线的多普勒频移来计算的,除了风场参数外,还可以探测温度、云顶高度和一些气溶胶特性。HRDI具有极高的光谱分辨率、较大的光通量和小的温度依赖性等优点^[145-146]。

多普勒非对称空间外差技术(DASH)的概念最早

由美国Englert团队^[147]在2006年提出,是一种全新的大气风场探测技术。DASH干涉仪与Michelson干涉仪在结构上相似,取消了动镜,故机械稳定性更高,构造紧凑,能够对多条谱线同时测量,反演风场精度较高^[148]。2019年8月基于该项技术全球高分辨率热层成像干涉仪(MIGHTI)搭载在ICON卫星上成功发射,成为国际上首个星载多普勒差分测风干涉仪。它拥有两个垂直视场,通过同时测量红色(630.03 nm)和绿色(557.73 nm)大气氧原子发射线多普勒频移来探测90~300 km高度区域的风速^[149]。为了验证MIGHTI的测量精度,Chen等^[150]利用武汉大学的流星雷达和水平风场模型(HWM14)的计算结果与2020年全年的ICON/MIGHTI卫星数据进行比较分析,结果表明,MIGHTI和他们都表现出强相关性。国外有报道用地基流星雷达和Fabry-Perot干涉仪同MIGHTI数据进行比较验证,在时空匹配大致的情况下结果都比较吻合^[151-152]。

4 主被动星载大气探测性能对比与分析

主被动星载大气探测性能对比与分析详见表3~6。

5 总结与展望

卫星遥感是获取全球范围大气参数的有效手段,为全球环境和气候变化提供科学数据支持。被动星载遥感发展起步时间较早,技术更加成熟,可探测的大气环境参数更加丰富,但被动遥感有着不可避免的劣势,如精度不高、高纬度地区覆盖不全、夜间探测数据缺乏等等。激光雷达作为典型的主动遥感设备,具有高精

表3 云遥感探测卫星载荷性能对比

Table 3 Comparison of cloud remote sensing satellite payload performance

Payload	Satellite	Active and passive	Advantage	Disadvantage
MERSI-II AGRI	Fengyun		With mature development, remote sensing instruments and inversion algorithms are diverse, and Fengyun satellite can form a network detection	Depending on sunlight, the temporal and spatial resolution is insufficient, the difference of the results of different algorithms is questionable, and the inversion effect is poor for complex cloud scenes
DPC	GF-5	Passive		
MODIS	Terra/Aqua			
AHI	Himawari			
CPR	CloudSat		Microwave radar can detect the vertical structure of thick clouds due to its strong penetration ability. Spaceborne Lidar has obvious advantages in retrieving cloud top height and high detection accuracy, and has unique advantages in macro and micro parameters of thin clouds	Microwave radar has low spatial resolution, low sensitivity to small-scale clouds, and does not have the detection ability from the ground to an altitude of 1 km, and the limited penetration ability of lidar makes it difficult to retrieve the height of the cloud base, and has limitations for the detection of thick clouds. The sky signal to noise ratio is low
CALIOP	CALIPSO	Active		
ACDL	DQ-1			

表4 大气气溶胶遥感探测卫星载荷性能对比
Table 4 Comparison of atmospheric aerosol remote sensing satellite payload performance

Payload	Satellite	Active and passive	Advantage	Disadvantage
AVHRR	NOAA			
DPC	GF-5			
MODIS	Terra/Aqua	Passive	Multi-spectral, multi-angle and polarization means, algorithms and instruments are diverse, the space coverage is large, and the retrievable aerosol parameters are numerous	Depending on sunlight, the spatial and temporal resolution is insufficient, the detection accuracy is limited, and the aerosol profile information cannot be provided
MISR	Terra			
GLAS	ICESat			
CALIOP	CALIPSO			
CATS	ISS	Active	It can detect aerosol by quantitative remote sensing, with high spatial and temporal resolution, provide global aerosol vertical structure and high detection accuracy. ACDL's HSRL system based on iodine filter can obtain aerosol information with higher accuracy without introducing Lidar ratio	CALIOP needs to assume Lidar ratios, increasing sources of error
ACDL	DQ-1			

表5 温室气体遥感探测卫星载荷性能对比
Table 5 Comparison of greenhouse gas remote sensing satellite payload performance

Payload	Satellite	Active and passive	Advantage	Disadvantage
SCIAMACHY	Envisat-1			
TANSO-FTS	GOSAT			
3-channel grating spectrometer	OCO	Passive	Various technologies, including Fourier interferometry, grating spectroscopy and space heterodyne spectroscopy technology, strong specialization, and there are specialized passive satellites to detect greenhouse gases, and a variety of observation modes, including nadir, flare, calibration, and target	Data validity is limited by clouds, aerosols, and latitude zones, surface reflectivity and atmospheric component scattering affect detection accuracy, and time and space are limited by night and north and south poles
ACGS	TANSAT			
GMI	GF-5			
ACDL	DQ-1	Active	High detection accuracy, CO ₂ detection is expected to achieve 1×10^{-6} accuracy, not easily affected by clouds and aerosols, can achieve all day observation, fill the gap of CO ₂ night observation, does not depend on the sun angle, the observation area covers the poles to achieve full latitude observation	The laser has high requirements and is difficult to develop, and the atmospheric parameters affect the high-precision inversion of greenhouse gases

度、高时空分辨率等优点,可弥补被动遥感的不足,目前地基和机载探测大气激光雷达已经相当成熟,星载激光雷达遥感探测是未来发展趋势,从LITE的发射到今天已经发展了近30年之久,可探测的大气参数主要包括云、气溶胶、温室气体、大气风场等。通过对比分析,揭示了大气环境参数主被动星载遥感探测技术的优缺点,从而可根据不同的应用场景和需求,选择合适的探测方式。

1)主被动联合观测、多组分同时测量将是未来全球大气参数探测的研究热点和发展趋势。主被动星载遥感仪器二者优势互补,可增加数据的有效性,实现更高精度的大气环境参数反演,同时增加数据的可对比

性。如我国即将发射的DQ-2卫星将激光雷达与高光谱技术结合,将会提高温室气体等参数的反演能力。多组分同时探测有效突破了单一组分探测的限制,可直接进行多参数同步反演。

2)发展全球大气环境参数和大气成分探测是星载激光雷达大气探测的重难点。如星载激光雷达探测大气风场只有ALADIN唯一的激光雷达载荷,虽然测风体制很多,但研制较为困难,国内还未研制出全球风场激光雷达遥感卫星。另外相对于被动卫星遥感来说,还未有专门的激光雷达载荷探测大气温度、湿度、密度和压强等参数,其次星载激光雷达探测大气成分方面需要完善,如未来我国发射高精度臭氧监测卫星搭载

表6 大气风场遥感探测卫星载荷性能对比

Table 6 Comparison of atmospheric wind field remote sensing satellite payload performance

Payload	Satellite	Active and passive	Advantage	Disadvantage
SEVIRII	MSG		Various detection techniques. The detection range is wide, including the atmospheric wind field in the mesosphere and most of the thermosphere height range. In the observation of tropospheric wind field, spaceborne passive remote sensing has reached the level of operational observation	
WINDII	UARS			
HRDI	UARS	Passive		The detection accuracy and spatial resolution are worse than that of active remote sensing
MIGHTI	ICON			
ALADIN	ADM-Aeolus	Active	It can provide the vertical profile of the global atmospheric wind field with high precision and high spatio-temporal resolution, and is one of the best means to obtain the three-dimensional global atmospheric wind field. There are many wind measurement systems that can be developed, and the development potential is great	The detection range is small, and the atmospheric wind profile in the global range of 0~25 km is detected. At present, there is only one kind of ALADIN, the system is single, and there is no Lidar wind measurement satellite in our country

臭氧探测激光雷达和宽波段高分辨偏振成像仪等4台遥感仪器,实现臭氧、PM_{2.5}和碳等参数的联合观测;增加甲烷、水汽等气体的探测。

3)一星多载荷以及多卫星组网探测是卫星遥感发展的趋势。将主被动载荷搭载在同一个卫星平台上不仅节省资源,同时提高反演的能力。建立高中低轨组网协同观测,低轨空间分辨率高,能够实现高精度观测,但是存在访问周期长的问题;高轨时间分辨率高,可进行高频次观测,能够实现连续观测,从而完善大气环境参数监测卫星体系。

4)开展新型激光遥感卫星研究。上海航天技术研究院联合中国科学院上海光学精密机械研究所、中国科学院安徽光学精密机械研究所等多家单位拟计划开展激光掩星星座大气观测,实现多类型大气成分垂直观测,进行全球温室气体和污染气体垂直廓线以及大气风速测量。飞秒光丝激光雷达遥感卫星利用飞秒激光大气非线性成丝效应实现紫外至可见宽谱段范围内的主动激光大气成分(O₃、SO₂、NO₂等)高精度探测,相对于被动探测方式来说,精度和垂直探测能力得到大幅提高,相对于传统激光探测,增加了探测谱段和气体种类。大力开展卫星遥感技术将为我国在国际上承担大国责任和增强外交话语权作出科技贡献。

参 考 文 献

- [1] 刘文清.“双碳”目标下大气环境光学监测技术发展机遇[J].光学学报, 2022, 42(6): 0600001.
Liu W Q. Opportunities and challenges for development of atmospheric environmental optics monitoring technique under “double carbon” goal[J]. Acta Optica Sinica, 2022, 42(6): 0600001.
- [2] Fan J W, Rosenfeld D, Yang Y, et al. Substantial contribution of anthropogenic air pollution to catastrophic floods in Southwest China[J]. Geophysical Research Letters, 2015, 42(14): 6066-6075.
- [3] 吴德伟, 景井, 李海林. 临近空间环境对高超声速飞行器导航系统的影响分析[J]. 飞航导弹, 2012(12): 73-80.
Wu D W, Jing J, Li H L. Analysis of influence of near space environment on navigation system of hypersonic vehicle[J]. Aerospace Technology, 2012(12): 73-80.
- [4] Liu D, Wang Z E, Liu Z Y, et al. A height resolved global view of dust aerosols from the first year CALIPSO lidar measurements[J]. Journal of Geophysical Research, 2008, 113(D16): D16214.
- [5] Sassen K, Wang Z, Liu D. Cirrus clouds and deep convection in the tropics: Insights from CALIPSO and CloudSat[J]. Journal of Geophysical Research, 2011, 116(D4): D00H06.
- [6] Kikon N, Kumar D, Ahmed S A. Spaceborne synthetic aperture radar (SAR) earth observations for surface deformation analysis and mapping[J]. Arabian Journal of Geosciences, 2022, 15(12): 1131.
- [7] 王晓海, 杨斌利. 国外星载微波散射计应用现状及未来发展趋势[J]. 中国航天, 2006(7): 26-29.
Wang X H, Yang B L. Application status and future development trend of spaceborne microwave scatterometer abroad[J]. Aerospace China, 2006(7): 26-29.
- [8] Sahak N, Asmat A, Hazali N A, et al. Multiangle Imaging Spectroradiometer (MISR) and Moderate Resolution Imaging Spectrometer (MODIS) Aerosol Optical Depth (AOD) spatial variations in Peninsular Malaysia[J]. IOP Conference Series: Earth and Environmental Science, 2019, 373: 012010.
- [9] Kristoffersen S K, Ward W E, Brown S, et al. Calibration and validation of the advanced E-Region Wind Interferometer[J]. Atmospheric Measurement Techniques, 2013, 6(7): 1761-1776.
- [10] Chen X, Yang D X, Cai Z N, et al. Aerosol retrieval sensitivity and error analysis for the cloud and aerosol polarimetric imager on board TanSat: the effect of multi-angle measurement[J]. Remote Sensing, 2017, 9(2): 183.
- [11] 田晓敏, 刘东, 徐继伟, 等. 大气探测激光雷达网络和星载激光雷达技术综述[J]. 大气与环境光学学报, 2018, 13(6): 401-416.
Tian X M, Liu D, Xu J W, et al. Review on atmospheric detection lidar network and spaceborne lidar technology[J]. Journal of Atmospheric and Environmental Optics, 2018, 13(6): 401-416.
- [12] 田晓敏, 刘东, 徐继伟, 等. 大气探测激光雷达技术综述[J]. 大气与环境光学学报, 2018, 13(5): 321-341.
Tian X M, Liu D, Xu J W, et al. Review of lidar technology for

- atmosphere monitoring[J]. *Journal of Atmospheric and Environmental Optics*, 2018, 13(5): 321-341.
- [13] Winker D M, Couch R H, McCormick M P. An overview of LITE: NASA's lidar in-space technology experiment[J]. *Proceedings of the IEEE*, 1996, 84(2): 164-180.
- [14] Osborn M T, Kent G S, Trepte C R. Stratospheric aerosol measurements by the lidar in space technology experiment[J]. *Journal of Geophysical Research: Atmospheres*, 1998, 103(D10): 11447-11453.
- [15] Menzies R T, Tratt D M, Hunt W H. Lidar in-space technology experiment measurements of sea surface directional reflectance and the link to surface wind speed[J]. *Applied Optics*, 1998, 37(24): 5550-5559.
- [16] Winker M D, Trepte R C. Laminar cirrus observed near the tropical tropopause by LITE[J]. *Geophysical Research Letters*, 1998, 25(17): 3351-3354.
- [17] Cuomo V, Girolamo D P, Pappalardo G, et al. Lidar in space technology experiment correlative measurements by lidar in Potenza, southern Italy[J]. *Journal of Geophysical Research*, 1998, 103(D10): 11455-11464.
- [18] Marini A. Atlid: the technology development programme for esa's satellite-borne atmospheric lidar[EB/OL]. [2023-02-03]. <https://www.esa.int/esapub/bulletin/bullet95/MARINI.pdf>.
- [19] Morancais D, Sesselmann R, Hueber M. Compact atmospheric LIDAR instrument (C-ATLID)[J]. *Proceedings of SPIE*, 1994, 33(14): 63-67.
- [20] Morancais D, Sesselmann R, Benedetti-Michelangeli G, et al. The atmospheric lidar instrument (ATLID) [J]. *Acta Astronautica*, 1994, 34: 63-67.
- [21] Hueber M F. ATLID: the European backscatter lidar development program[J]. *Proceedings of SPIE*, 1994, 2310: 34-42.
- [22] Barker H W, Jerg M P, Wehr T, et al. A 3D cloud-construction algorithm for the EarthCARE satellite mission[J]. *Quarterly Journal of the Royal Meteorological Society*, 2011, 137(657): 1042-1058.
- [23] Lefebvre A, Hélière A, Albiñana A P, et al. EarthCARE mission, overview, implementation approach, and development status[J]. *Proceedings of SPIE*, 2014, 9264: 926403.
- [24] EarthCARE-Earth Online[EB/OL]. [2023-03-04]. <https://earth.esa.int/eogateway/missions/earthcare>.
- [25] The Geoscience Laser Altimeter System (GLAS) [EB/OL]. [2023-03-04]. <https://attic.gsfc.nasa.gov/glas/index.html>.
- [26] Spinhirne J D, Palm S P, Hart W D, et al. Cloud and aerosol measurements from GLAS: overview and initial results[J]. *Geophysical Research Letters*, 2005, 32(22): L22S03.
- [27] Schutz B E, Zwally H J, Shuman C A, et al. Overview of the ICESat mission[J]. *Geophysical Research Letters*, 2005, 32(21): L21S01.
- [28] Abshore J B, Sun X L, Riris H, et al. Geoscience Laser Altimeter System (GLAS) on the ICESat Mission: on-orbit measurement performance[J]. *Geophysical Research Letters*, 2005, 32(21): L21S02.
- [29] Hlavka D L, Palm S P, Hart W D, et al. Aerosol and cloud optical depth from GLAS: results and verification for an October 2003 California fire smoke case[J]. *Geophysical Research Letters*, 2005, 32(22): L22S07.
- [30] Hart W D, Spinhirne J D, Palm S P, et al. Height distribution between cloud and aerosol layers from the GLAS spaceborne lidar in the Indian Ocean region[J]. *Geophysical Research Letters*, 2005, 32(22): L22S06.
- [31] Martino A J, Neumann T A, Kurtz N T, et al. ICESat-2 mission overview and early performance[J]. *Proceedings of SPIE*, 2019, 11151: 111510C.
- [32] Magruder L, Neumann T, Kurtz N. ICESat-2 early mission synopsis and observatory performance[J]. *Earth and Space Science*, 2021, 8(5): e2020EA001555.
- [33] Palm S P, Yang Y K, Herzfeld U, et al. ICESat-2 atmospheric channel description, data processing and first results[J]. *Earth and Space Science*, 2021, 8(8): e2020EA001470.
- [34] Markus T, Neumann T, Martino A, et al. The Ice, Cloud, and land Elevation Satellite-2 (ICESat-2): science requirements, concept, and implementation[J]. *Remote Sensing of Environment*, 2017, 190: 260-273.
- [35] Winker D M, Vaughan M A, Omar A, et al. Overview of the CALIPSO mission and CALIOP data processing algorithms[J]. *Journal of Atmospheric and Oceanic Technology*, 2009, 26(11): 2310-2323.
- [36] Winker D, Vaughan M, Hunt B. The CALIPSO mission and initial results from CALIOP[J]. *Proceedings of SPIE*, 2006, 6409: 640902.
- [37] Winker D M, Pelon J R, McCormick M P. CALIPSO mission: spaceborne lidar for observation of aerosols and clouds[J]. *Proceedings of SPIE*, 2003, 4893: 1-11.
- [38] Hunt W H, Winker D M, Vaughan M A, et al. CALIPSO lidar description and performance assessment[J]. *Journal of Atmospheric and Oceanic Technology*, 2009, 26(7): 1214-1228.
- [39] Winker D M, Hunt W H, Hostetler C A. Status and performance of the CALIOP lidar[J]. *Proceedings of SPIE*, 2004, 5575: 8-15.
- [40] Maria M S, Winker D. Applications of theoretical optical parameters from a transport model to the quantification and qualification of aerosol populations of a lidar in space data retrieval[J]. *Proceedings of SPIE*, 2004, 5240: 235-242.
- [41] 王帅辉, 韩志刚, 姚志刚, 等. 基于CloudSat资料的中国及周边地区云垂直结构统计分析[J]. *高原气象*, 2011, 30(1): 38-52.
- Wang S H, Han Z G, Yao Z G, et al. Analysis on cloud vertical structure over China and its neighborhood based on CloudSat data[J]. *Plateau Meteorology*, 2011, 30(1): 38-52.
- [42] 张华, 彭杰, 荆现文, 等. 东亚地区云的垂直重叠特性及其对云辐射强迫的影响[J]. *中国科学: 地球科学*, 2013, 43(4): 523-535.
- Zhang H, Peng J, Jing X W, et al. Vertical overlapping characteristics of clouds in East Asia and its influence on cloud radiation forcing[J]. *Scientia Sinica: Terra*, 2013, 43(4): 523-535.
- [43] 杨冰韵, 张华, 彭杰, 等. 利用CloudSat卫星资料分析云微物理和光学性质的分布特征[J]. *高原气象*, 2014, 33(4): 1105-1118.
- Yang B Y, Zhang H, Peng J, et al. Analysis on global distribution characteristics of cloud microphysical and optical properties based on the CloudSat data[J]. *Plateau Meteorology*, 2014, 33(4): 1105-1118.
- [44] 李积明, 黄建平, 衣育红, 等. 利用星载激光雷达资料研究东亚地区云垂直分布的统计特征[J]. *大气科学*, 2009, 33(4): 698-707.
- Li J M, Huang J P, Yi Y H, et al. Using spaceborne lidar data to study the statistical characteristics of cloud vertical distribution in East Asia[J]. *Chinese Journal of Atmospheric Sciences*, 2009, 33(4): 698-707.
- [45] Sassen K, Wang Z E, Liu D. Global distribution of cirrus clouds from CloudSat/Cloud-Aerosol Lidar and Infrared Pathfinder Satellite Observations (CALIPSO) measurements[J]. *Journal of Geophysical Research*, 2008, 113(D8): D00A12.
- [46] 郑建宇, 刘东, 王志恩, 等. CloudSat/CALIPSO卫星资料分析云的全球分布及其季节变化特征[J]. *气象学报*, 2018, 76(3): 420-433.
- Zheng J Y, Liu D, Wang Z E, et al. Global distribution and seasonal variation of clouds observed from CloudSat/CALIPSO [J]. *Acta Meteorologica Sinica*, 2018, 76(3): 420-433.
- [47] Zheng J Y, Liu D, Wang Z E, et al. Differences among three types of tropical deep convective clusters observed from A-Train satellites[J]. *Journal of Quantitative Spectroscopy and Radiative Transfer*, 2018, 217: 253-261.

- [48] Omar A H, Winker D M, Vaughan M A, et al. The CALIPSO automated aerosol classification and lidar ratio selection algorithm [J]. *Journal of Atmospheric and Oceanic Technology*, 2009, 26(10): 1994-2014.
- [49] de Oliveira A M, Souza C T, de Oliveira N P M, et al. Analysis of atmospheric aerosol optical properties in the northeast Brazilian atmosphere with remote sensing data from MODIS and CALIOP/CALIPSO satellites, AERONET photometers and a ground-based lidar[J]. *Atmosphere*, 2019, 10(10): 594.
- [50] 孙雨辰. 基于星载激光雷达的全球气溶胶光学特性研究[D]. 青岛: 中国海洋大学, 2014.
- Sun Y C. Study on global aerosol optical characteristics based on spaceborne lidar[D]. Qingdao: Ocean University of China, 2014.
- [51] 张馨毅, 吴东, 杨振威, 等. 星载激光雷达数据海面风速反演模型研究[J]. 光学学报, 2022, 42(18): 1828007.
- Zhang X Y, Wu D, Yang Z W, et al. Research on inversion model of sea surface wind speed from spaceborne lidar data[J]. *Acta Optica Sinica*, 2022, 42(18): 1828007.
- [52] 韩延磊. SAR 和 CALIPSO 数据反演海面风速[D]. 青岛: 中国海洋大学, 2010.
- Han Y L. Retrieval of sea surface wind speed from SAR and CALIPSO data[D]. Qingdao: Ocean University of China, 2010.
- [53] 张小雪. 提高星载激光雷达海面风速探测精度的研究[D]. 青岛: 中国海洋大学, 2012.
- Zhang X X. Research on improving the detection accuracy of sea surface wind speed by spaceborne lidar[D]. Qingdao: Ocean University of China, 2012.
- [54] CATS: cloud-aerosol transport system | NASA[EB/OL]. [2023-03-04]. <https://www.nasa.gov/cats>.
- [55] Pauly R M, Yorks J E, Hlavka D L, et al. Cloud-aerosol transport system (CATS) 1064 nm calibration and validation[J]. *Atmospheric Measurement Techniques*, 2019, 12(11): 6241-6258.
- [56] Yorks J E, McGill M J, Palm S P, et al. An overview of the CATS level 1 processing algorithms and data products[J]. *Geophysical Research Letters*, 2016, 43(9): 4632-4639.
- [57] Lee L, Zhang J L, Reid J S, et al. Investigation of CATS aerosol products and application toward global diurnal variation of aerosols[J]. *Atmospheric Chemistry and Physics*, 2019, 19(19): 12687-12707.
- [58] Pauly R M, Yorks J E, Hlavka D L, et al. Cloud-aerosol transport system (CATS) 1064 nm calibration and validation[J]. *Atmospheric Measurement Techniques*, 2019, 12(11): 6241-6258.
- [59] 宋晶晶. 首个星载全球大气风场激光雷达成功发射[J]. 国际太空, 2018(9): 40-43.
- Song J J. The first spaceborne global atmospheric wind lidar was successfully launched[J]. *Space International*, 2018(9): 40-43.
- [60] 陈炳龙, 杨忠东, 闵敏, 等. 星载多普勒测风激光雷达应用需求与研究进展[J]. 激光与光电子学进展, 2020, 57(19): 190003.
- Chen B L, Yang Z D, Min M, et al. Application requirements and research progress of spaceborne Doppler wind lidar[J]. *Laser & Optoelectronics Progress*, 2020, 57(19): 190003.
- [61] Rohaly G D, Krishnamurti T N. An observing system simulation experiment for the laser atmospheric wind sounder (LAWS)[J]. *Journal of Applied Meteorology*, 1993, 32(9): 1453-1471.
- [62] Phillips M W, Schnal D L, Hale C P, et al. Design and development of the SPARCLE coherent lidar transceiver[J]. *Proceedings of SPIE*, 1999, 3707: 256-267.
- [63] Itabe T, Mizutani K. Coherent Doppler wind lidar for the Japanese experimental module of the ISS[C]//Optical Remote Sensing, February 3, 2003, Québec City, Canada. Washington, D.C.: Optica Publishing Group, 2003: OWA1.
- [64] Emmitt G D. Combining direct and coherent detection for Doppler wind lidar[J]. *Proceedings of SPIE*, 2004, 5575: 31-37.
- [65] Kanitz T, Wernham D, Alvarez E, et al. Aeolus - ESA'S wind lidar mission, a brief status[C]//IGARSS 2020-2020 IEEE International Geoscience and Remote Sensing Symposium, September 26-October 2, 2020, Waikoloa, HI, USA. New York: IEEE Press, 2021: 3463-3466.
- [66] Straume A G, Elfving A, Wernham D, et al. ESA's spaceborne lidar mission ADM-aeolus; recent achievements and preparations for launch[J]. *EPJ Web of Conferences*, 2016, 119: 01001.
- [67] 陈卫标, 刘继桥, 侯霞, 等. 大气环境监测卫星激光雷达技术[J]. 上海航天(中英文), 2023, 40(3): 13-20, 110.
- Chen W B, Liu J Q, Hou X, et al. Lidar technology for atmosphere environment monitoring satellite[J]. *Aerospace Shanghai (Chinese & English)*, 2023, 40(3): 13-20, 110.
- [68] 刘东, 陈斯健, 刘群, 等. 星载环境探测激光雷达及其关键技术[J]. 光学学报, 2022, 42(17): 1701001.
- Liu D, Chen S J, Liu Q, et al. Spaceborne environmental detection lidar and its key techniques[J]. *Acta Optica Sinica*, 2022, 42(17): 1701001.
- [69] 星载大气探测激光雷达[EB/OL]. [2023-02-03]. <http://www.siom.cas.cn/acdl>. ACDL[EB/OL]. [2023-02-03]. <http://www.siom.cas.cn/acdl>.
- [70] 贺涛, 国爱燕, 黄缙, 等. 陆地生态系统碳监测卫星“句芒”号概览[J]. 国际太空, 2022(9): 8-12.
- He T, Guo A Y, Huang J, et al. Overview of terrestrial ecosystem carbon monitoring satellite “ju Mang” [J]. *Space International*, 2022(9): 8-12.
- [71] 孙立, 杨居奎, 王玉诏, 等. 主被动一体化多波束激光雷达设计与实现[J]. 航天返回与遥感, 2022, 43(6): 27-35.
- Sun L, Yang J K, Wang Y Z, et al. Design and implementation of active and passive integrated multi-beam lidar[J]. *Spacecraft Recovery & Remote Sensing*, 2022, 43(6): 27-35.
- [72] 汤天瑾, 杨居奎, 伏瑞敏, 等. 陆地生态系统碳监测卫星多波束激光雷达光学系统设计[J]. 航天返回与遥感, 2022, 43(6): 36-49.
- Tang T J, Yang J K, Fu R M, et al. Optical system design of multi-beam lidar for terrestrial ecosystem carbon monitoring satellite[J]. *Spacecraft Recovery & Remote Sensing*, 2022, 43(6): 36-49.
- [73] Du S S, Liu X J, Chen J D, et al. Prospects for solar-induced chlorophyll fluorescence remote sensing from the SIFIS payload onboard the TECIS-1 satellite[J]. *Journal of Remote Sensing*, 2022, 2022: 9845432.
- [74] Durden S L, Tanelli S, Epp L, et al. A cloud and precipitation radar system concept for the ACE mission[EB/OL]. [2023-02-03]. http://vigr.missouri.edu/~gdesouza/Research/Conference_CDs/IGARSS_2010/pdfs/2019.pdf.
- [75] Starr D. NASA's aerosol-cloud-ecosystems (ACE) mission[C]//Imaging and Applied Optics, July 10-14, 2011, Toronto, Canada. Washington, D. C.: Optica Publishing Group, 2011: HMA4.
- [76] Jamnejad V, Long E, Durden S. Design of a quasi optical transmission line for Cloud and precipitation radar system of ACE mission[C]//2015 IEEE Aerospace Conference, March 7-14, 2015, Big Sky, MT, USA. New York: IEEE Press, 2015.
- [77] Singh U, Yu J R, Petros M, et al. Development of a pulsed 2-micron integrated path differential absorption lidar for CO₂ measurement[J]. *Proceedings of SPIE*, 2013, 8872: 887209.
- [78] Abshire J, Ramanathan A, Riris H, et al. Airborne measurements of CO₂ column concentration and range using a pulsed direct-detection IPDA lidar[J]. *Remote Sensing*, 2013, 6(1): 443-469.
- [79] Refaat T F, Singh U N, Yu J R, et al. Evaluation of an airborne triple-pulsed 2 μm IPDA lidar for simultaneous and independent atmospheric water vapor and carbon dioxide measurements[J]. *Applied Optics*, 2015, 54(6): 1387-1398.
- [80] Refaat T F, Singh U N, Yu J R, et al. Double-pulse 2-μm

- integrated path differential absorption lidar airborne validation for atmospheric carbon dioxide measurement[J]. *Applied Optics*, 2016, 55(15): 4232-4246.
- [81] Abshire J B, Riris H, Allan G R, et al. A lidar approach to measure CO₂ concentrations from space for the ASCENDS mission[J]. *Proceedings of SPIE*, 2010, 7832: 78320D.
- [82] Caron J, Durand Y. Operating wavelengths optimization for a spaceborne lidar measuring atmospheric CO₂[J]. *Applied Optics*, 2009, 48(28): 5413-5422.
- [83] Caron J, Durand Y, Bezy J L, et al. Performance modeling for A-Scope: a space-borne lidar measuring atmospheric CO₂[J]. *Proceedings of SPIE*, 2009, 7479: 74790E.
- [84] Kaminski T, Scholze M, Houweling S. Quantifying the benefit of A-Scope data for reducing uncertainties in terrestrial carbon fluxes in CCDAS[J]. *Tellus B: Chemical and Physical Meteorology*, 2010, 62(5): 784-796.
- [85] Pierangelo C, Millet B, Esteve F, et al. MERLIN (methane remote sensing lidar mission): an overview[J]. *EPJ Web of Conferences*, 2016, 119: 26001.
- [86] Ehret G, Bousquet P, Pierangelo C, et al. MERLIN: a french-german space lidar mission dedicated to atmospheric methane[J]. *Remote Sensing*, 2017, 9(10): 1052.
- [87] Kiemle C, Kawa S R, Quatrefavet M, et al. Performance simulations for a spaceborne methane lidar mission[J]. *Journal of Geophysical Research: Atmospheres*, 2014, 119(7): 4365-4379.
- [88] Vaughan W W, Johnson D L. Meteorological satellites—the very early years prior to launch of TIROS-I[J]. *Bulletin of the American Meteorological Society*, 1994, 75(12): 2295-2302.
- [89] 张鹏, 杨军, 关敏, 等. WMO空间计划与风云气象卫星的国际化发展趋势[J]. 气象科技进展, 2022, 12(5): 56-63, 79.
Zhang P, Yang J, Guan M, et al. WMO space plan and the international development trend of Fengyun meteorological satellite[J]. *Advances in Meteorological Science and Technology*, 2022, 12(5): 56-63, 79.
- [90] 尚华哲, 胡斯勒图, 李明, 等. 基于被动遥感卫星可见至红外通道观测的云特性遥感[J]. 光学学报, 2022, 42(6): 0600003.
Shang H Z, Husi L T, Li M, et al. Remote sensing of cloud properties based on visible-to-infrared channel observation from passive remote sensing satellites[J]. *Acta Optica Sinica*, 2022, 42(6): 0600003.
- [91] 张森, 徐娜, 郑照军, 等. FY-3D MERSI-II 云顶产品算法及精度检验[J]. 热带气象学报, 2022, 38(6): 779-786.
Zhang M, Xu N, Zheng Z J, et al. Algorithm and accuracy test of FY-3D MERSI-II genting product[J]. *Journal of Tropical Meteorology*, 2022, 38(6): 779-786.
- [92] 张志清, 陆风, 方翔, 等. FY-4 卫星应用和发展[J]. 上海航天, 2017, 34(4): 8-19.
Zhang Z Q, Lu F, Fang X, et al. Application and development of FY-4 meteorological satellite[J]. *Aerospace Shanghai*, 2017, 34(4): 8-19.
- [93] Pilewskie P, Twomey S. Cloud phase discrimination by reflectance measurements near 1.6 and 2.2 μm[J]. *Journal of the Atmospheric Sciences*, 1987, 44(22): 3419-3420.
- [94] 袁锦涵, 周永波, 刘玉宝, 等. 云滴谱分布对FY-4A/AGRI水云光学厚度与有效粒子半径反演的影响[J]. 光学学报, 2022, 42(6): 0628004.
Yuan J H, Zhou Y B, Liu Y B, et al. Effect of cloud droplet spectrum distribution on retrievals of water cloud optical thickness and effective particle radius by AGRI onboard FY-4A satellite[J]. *Acta Optica Sinica*, 2022, 42(6): 0628004.
- [95] 陈良富, 尚华哲, 范萌, 等. 高分五号卫星大气参数探测综述[J]. 遥感学报, 2021, 25(9): 1917-1931.
Chen L F, Shang H Z, Fan M, et al. Mission overview of the GF-5 satellite for atmospheric parameter monitoring[J]. *National Remote Sensing Bulletin*, 2021, 25(9): 1917-1931.
- [96] Deschamps P Y, Breon F M, Leroy M, et al. The POLDER mission: instrument characteristics and scientific objectives[J]. *IEEE Transactions on Geoscience and Remote Sensing*, 1994, 32(3): 598-615.
- [97] 常钰阳, 孙斌, 黄禅, 等. 多角度偏振云检测及云参数反演[J]. 光学学报, 2020, 40(11): 1101002.
- [98] Chang Y Y, Sun B, Huang C, et al. Cloud detection and parameter inversion using multi-directional polarimetric observations[J]. *Acta Optica Sinica*, 2020, 40(11): 1101002.
- [99] Li C, Ma J J, Yang P, et al. Detection of cloud cover using dynamic thresholds and radiative transfer models from the polarization satellite image[J]. *Journal of Quantitative Spectroscopy and Radiative Transfer*, 2019, 222/223: 196-214.
- [100] Platnick S, King M D, Ackerman S A, et al. The MODIS cloud products: algorithms and examples from Terra[J]. *IEEE Transactions on Geoscience and Remote Sensing*, 2003, 41(2): 459-473.
- [101] Platnick S, Meyer K G, King M D, et al. The MODIS cloud optical and microphysical products: collection 6 updates and examples from terra and aqua[J]. *IEEE Transactions on Geoscience and Remote Sensing*, 2017, 55(1): 502-525.
- [102] Wylie D P, Menzel W P. Eight years of high cloud statistics using HIRS[J]. *Journal of Climate*, 1999, 12(1): 170-184.
- [103] Wylie D P, Menzel W P, Woolf H M, et al. Four years of global cirrus cloud statistics using HIRS[J]. *Journal of Climate*, 1994, 7(12): 1972-1986.
- [104] Platnick S, Meyer K, Wind G, et al. The NASA MODIS-VIIRS continuity cloud optical properties products[J]. *Remote Sensing*, 2020, 13(1): 2.
- [105] Iwabuchi H, Putri N S, Saito M, et al. Cloud property retrieval from multiband infrared measurements by himawari-8[J]. *Journal of the Meteorological Society of Japan Ser II*, 2018, 96B: 27-42.
- [106] 丁宁, 于博, 颜昌翔, 等. 星载气溶胶被动光学遥感仪器:进展与未来展望[J]. 光学学报, 2022, 42(17): 1701002.
Ding N, Yu B, Yan C X, et al. Spaceborne aerosol passive optical remote sensing instrument: progress and future prospect [J]. *Acta Optica Sinica*, 2022, 42(17): 1701002.
- [107] 张军强, 薛闯, 高志良, 等. 云与气溶胶光学遥感仪器发展现状及趋势[J]. 中国光学, 2015, 8(5): 679-698.
Zhang J Q, Xue C, Gao Z L, et al. Optical remote sensor for cloud and aerosol from space: past, present and future[J]. *Chinese Optics*, 2015, 8(5): 679-698.
- [108] Rao C R N, Stowe L L, McClain E P. Remote sensing of aerosols over the oceans using AVHRR data Theory, practice and applications[J]. *International Journal of Remote Sensing*, 1989, 10(4/5): 743-749.
- [109] Zhao B L, Yu X D. Investigation of the aerosol optical thickness on ocean surface by satellite remote sensing[J]. *Science Bulletin*, 1987, 32(17): 1183-1187.
- [110] Mishchenko M I, Geogdzhayev I V, Cairns B, et al. Aerosol retrievals over the ocean by use of channels 1 and 2 AVHRR data: sensitivity analysis and preliminary results[J]. *Applied Optics*, 1999, 38(36): 7325-7341.
- [111] Hauser A, Oesch D, Foppa N, et al. NOAA AVHRR derived aerosol optical depth over land[J]. *Journal of Geophysical Research*, 2005, 110(D8): D08204.
- [112] 高玲, 张里阳, 李俊, 等. 利用AVHRR数据反演陆地气溶胶光学厚度[J]. 应用气象学报, 2014, 25(1): 42-51.
Gao L, Zhang L Y, Li J, et al. Retrieval of atmospheric aerosol optical depth over land from AVHRR[J]. *Journal of Applied Meteorological Science*, 2014, 25(1): 42-51.
- [113] Wei J, Li Z Q, Peng Y R, et al. MODIS Collection 6.1 aerosol optical depth products over land and ocean: validation and comparison[J]. *Atmospheric Environment*, 2019, 201: 428-440.
- [114] 毛节泰, 李成才, 张军华, 等. MODIS卫星遥感北京地区气溶胶光学厚度及与地面光度计遥感的对比[J]. 应用气象学报, 2002, 13(S1): 127-135.
- [115] Mao J T, Li C C, Zhang J H, et al. The comparison of remote sensing aerosol optical depth from modis data and ground Sun-

- photometer observations[J]. *Quarterly Journal of Applied Meteorology*, 2002, 13(S1): 127-135.
- [114] Wei J, Li Z Q, Sun L, et al. MODIS Collection 6.1 3 km resolution aerosol optical depth product: global evaluation and uncertainty analysis[J]. *Atmospheric Environment*, 2020, 240: 117768.
- [115] 苏明宇, 刘华柏, 阳艾利, 等. 中国不同气候区域MODIS C6.1气溶胶光学厚度产品的验证及对比分析[J]. *环境科学学报*, 2023, 43(6): 11-26.
- Su Y Y, Liu H B, Yang A L, et al. Evaluation and comparative analysis for the MODIS C6.1 aerosol optical depth products in different climate regions over China[J]. *Acta Scientiae Circumstantiae*, 2023, 43(6): 11-26.
- [116] Liu Y, Franklin M, Kahn R, et al. Using aerosol optical thickness to predict ground-level PM_{2.5} concentrations in the St. Louis area: a comparison between MISR and MODIS[J]. *Remote Sensing of Environment*, 2007, 107(1/2): 33-44.
- [117] Zhang J, Reid J S. A decadal regional and global trend analysis of the aerosol optical depth using a data-assimilation grade over-water MODIS and Level 2 MISR aerosol products[J]. *Atmospheric Chemistry and Physics*, 2010, 10(22): 10949-10963.
- [118] Kahn R A, Gaitley B J. An analysis of global aerosol type as retrieved by MISR[J]. *Journal of Geophysical Research: Atmospheres*, 2015, 120(9): 4248-4281.
- [119] Kahn R A, Nelson D L, Garay M J, et al. MISR aerosol product attributes and statistical comparisons with MODIS[J]. *IEEE Transactions on Geoscience and Remote Sensing*, 2009, 47(12): 4095-4114.
- [120] 张艳婷, 陈斌, 张廷瀚, 等. 利用MODIS和MISR资料对APEC会议期间气溶胶时空分布特征的分析[J]. *大气与环境光学学报*, 2017, 12(2): 136-147.
- Zhang Y T, Chen B, Zhang T H, et al. Analysis of the spatiotemporal variations of aerosols during APEC using MODIS and MISR data[J]. *Journal of Atmospheric and Environmental Optics*, 2017, 12(2): 136-147.
- [121] Li Z Q, Hou W Z, Hong J, et al. Directional Polarimetric Camera (DPC): monitoring aerosol spectral optical properties over land from satellite observation[J]. *Journal of Quantitative Spectroscopy and Radiative Transfer*, 2018, 218: 21-37.
- [122] 李正强, 谢一淞, 石玉胜, 等. 大气环境卫星温室气体和气溶胶协同观探测综述[J]. *遥感学报*, 2022, 26(5): 795-816.
- Li Z Q, Xie Y S, Shi Y S, et al. A review of collaborative remote sensing observation of greenhouse gases and aerosol with atmospheric environment satellites[J]. *National Remote Sensing Bulletin*, 2022, 26(5): 795-816.
- [123] 提汝芳, 樊依哲, 黄红莲, 等. 基于高分五号卫星DPC和AERONET站点数据的地表BPDF模型对比分析[J]. *光学学报*, 2022, 42(18): 1828003.
- Ti R F, Fan Y Z, Huang H L, et al. Comparative analysis of BPDF land surface models based on DPC measurements of Gaofen-5 satellite and data of AERONET sites[J]. *Acta Optica Sinica*, 2022, 42(18): 146-154.
- [124] Li L, Che H Z, Zhang X D, et al. A satellite-measured view of aerosol component content and optical property in a haze-polluted case over North China Plain[J]. *Atmospheric Research*, 2022, 266: 105958.
- 杨晓钰, 王中挺, 潘光, 等. 卫星遥感温室气体的大气观测技术进展[J]. *大气与环境光学学报*, 2022, 17(6): 581-597.
- Yang X Y, Wang Z T, Pan G, et al. Progress in atmospheric observation technology of greenhouse gases by satellite remote sensing[J]. *Journal of Atmospheric and Environmental Optics*, 2022, 17(6): 581-597.
- [125] 刘毅, 王婧, 车舸, 等. 温室气体的卫星遥感: 进展与趋势[J]. *遥感学报*, 2021, 25(1): 53-64.
- Liu Y, Wang J, Che K, et al. Satellite remote sensing of greenhouse gases: progress and trends[J]. *National Remote Sensing Bulletin*, 2021, 25(1): 53-64.
- [127] Kobayashi H, Shimota A, Yoshigahara C, et al. Satellite-borne high-resolution FTIR for lower atmosphere sounding and its evaluation[J]. *IEEE Transactions on Geoscience and Remote Sensing*, 1999, 37(3): 1496-1507.
- [128] Nakajima M, Suto H, Yotsutomo K, et al. Fourier transform spectrometer on GOSAT and GOSAT-2[J]. *Proceedings of SPIE*, 2017, 10563: 105634O.
- [129] Noël S, Bramstedt K, Hilker M, et al. Stratospheric CH₄ and CO₂ profiles derived from SCIAMACHY solar occultation measurements[J]. *Atmospheric Measurement Techniques*, 2016, 9(4): 1485-1503.
- [130] Frankenberg C, Aben I, Bergamaschi P, et al. Global column-averaged methane mixing ratios from 2003 to 2009 as derived from SCIAMACHY: trends and variability[J]. *Journal of Geophysical Research*, 2011, 116(D4): D04302.
- [131] Crisp D, Pollock H R, Rosenberg R, et al. The on-orbit performance of the Orbiting Carbon Observatory-2 (OCO-2) instrument and its radiometrically calibrated products[J]. *Atmospheric Measurement Techniques*, 2017, 10(1): 59-81.
- [132] Wunch E, Wennberg P O, Osterman G, et al. Comparisons of the orbiting carbon observatory-2 (OCO-2) XCO₂ measurements with TCCON[J]. *Atmospheric Measurement Techniques*, 2017, 10(6): 2209-2238.
- [133] Eldering A, Taylor T E, O'dell C W, et al. The OCO-3 mission: measurement objectives and expected performance based on 1 year of simulated data[J]. *Atmospheric Measurement Techniques*, 2019, 12(4): 2341-2370.
- [134] Yang D X, Liu Y, Feng L, et al. The first global carbon dioxide flux map derived from TanSat measurements[J]. *Advances in Atmospheric Sciences*, 2021, 38(9): 1433-1443.
- [135] Liu Y, Wang J, Yao L, et al. The TanSat mission: preliminary global observations[J]. *Science Bulletin*, 2018, 63(18): 1200-1207.
- [136] 熊伟.“高分五号”卫星大气主要温室气体监测仪(特邀)[J]. *红外与激光工程*, 2019, 48(3): 24-30.
- Xiong W. Greenhouse gases Monitoring Instrument(GMI) on GF-5 satellite (invited) [J]. *Infrared and Laser Engineering*, 2019, 48(3): 24-30.
- [137] 李勤勤, 王先华, 叶函函, 等. 大气CO₂反演误差分析与精度验证[J]. *光学学报*, 2020, 40(6): 0601003.
- Li Q Q, Wang X H, Ye H H, et al. Atmospheric CO₂ inversion error analysis and accuracy verification[J]. *Acta Optica Sinica*, 2020, 40(6): 0601003.
- [138] 冯玉涛, 傅頤, 赵增亮, 等. 星载被动光学遥感大气风场探测技术进展综述[J]. *光学学报*, 2023, 43(6): 0601011.
- Feng Y T, Fu D, Zhao Z L, et al. An overview of spaceborne atmospheric wind field measurement with passive optical remote sensing[J]. *Acta Optica Sinica*, 2023, 43(6): 0601011.
- [139] Pasternak F, Hollier P, SEVIRIjouan J, the new imager for Meteosat second generation[C]//Proceedings of IGARSS '93 - IEEE International Geoscience and Remote Sensing Symposium, August 18-21, 1993, Tokyo, Japan. New York: IEEE Press, 2002: 1094-1099.
- [140] Nerushov A F, Kramchaninova E K. Method for determining atmospheric motion characteristics using measurements on geostationary meteorological satellites[J]. *Izvestiya, Atmospheric and Oceanic Physics*, 2011, 47(9): 1104-1113.
- [141] 韩威华, 王咏梅, 吕建工, 等. 中高层大气风场星载FPI干涉条纹的处理[J]. *科学技术与工程*, 2010, 10(10): 2420-2423.
- Han W H, Wang Y M, Lü J G, et al. Auto-processing of middle and upper atmosphere wind FPI interference fringe pattern[J]. *Science Technology and Engineering*, 2010, 10(10): 2420-2423.
- [142] Gault W A, Brun J F, Desaulniers M D L, et al. Design and on-orbit performance of the WINDII baffle system[J]. *Proceedings of SPIE*, 1993, 1753: 189-195.

- [143] Shepherd G G. Application of Doppler Michelson imaging to upper atmospheric wind measurement: WINDII and beyond[J]. *Applied Optics*, 1996, 35(16): 2764-2773.
- [144] Grassl H J, Skinner W R, Hays P B, et al. Atmospheric wind measurements with the high-resolution Doppler imager[J]. *Journal of Spacecraft and Rockets*, 1995, 32(1): 169-176.
- [145] Hays P B, Team H S. Remote sensing of mesospheric winds with the high-resolution Doppler imager[J]. *Planetary and Space Science*, 1992, 40(12): 1599-1606.
- [146] Hays P B, Abreu V J, Dobbs M E, et al. The high-resolution Doppler imager on the upper atmosphere research satellite[J]. *Journal of Geophysical Research*, 1993, 98(D6): 10713-10723.
- [147] Englert C R, Harlander J M, Babcock D D, et al. Doppler asymmetric spatial heterodyne spectroscopy (DASH): an innovative concept for measuring winds in planetary atmospheres [J]. *Proceedings of SPIE*, 2006, 6303: 63030T.
- [148] 于婷婷. 多普勒差分干涉仪干涉图预处理关键环节研究[D]. 西安: 中国科学院西安光学精密机械研究所, 2020.
Yu T T. Research on key steps of interferogram preprocessing for Doppler asymmetric spatial heterodyne interferometer[D].
- [149] Xi'an: Xi'an Institute of Optics and Precision Mechanics, Chinese Academy of Sciences, 2020.
- [150] Marr K D, Morrow W H, Brown C M, et al. Calibration lamp design, characterization, and implementation for the Michelson Interferometer for Global High-Resolution Thermospheric Imaging instrument on the Ionospheric Connection satellite[J]. *Optical Engineering*, 2019, 58(5): 054104.
- [151] Chen Z, Liu Y, Du Z T, et al. Validation of MIGHTI/ICON atmospheric wind observations over China region based on meteor radar and horizontal wind model (HWM14) [J]. *Atmosphere*, 2022, 13(7): 1078.
- [152] Harding B J, Chau J L, He M S, et al. Validation of ICON-MIGHTI thermospheric wind observations: 2. green-line comparisons to specular meteor radars[J]. *Journal of Geophysical Research: Space Physics*, 2021, 126(3): e2020JA028947.
- [153] Makela J J, Baughman M, Navarro L A, et al. Validation of ICON-MIGHTI thermospheric wind observations: 1. nighttime red-line ground-based Fabry-Perot interferometers[J]. *Journal of Geophysical Research: Space Physics*, 2021, 126(2): e2020JA028726.

Comparison and Analysis of Payloads Performance for Active and Passive Spaceborne Atmospheric Detection

Wang Jingsong^{1,3}, Liu Dong^{1,2*}

¹*Key Laboratory of Atmospheric Optics, Anhui Institute of Optics and Fine Mechanics, Hefei Institutes of Physical Science, Chinese Academy of Sciences, Hefei 230031, Anhui, China;*

²*Advanced Laser Technology Laboratory of Anhui Province, Hefei 230037, Anhui, China;*

³*Science Island Branch of Graduate School, University of Science and Technology of China, Hefei 230026, Anhui, China*

Abstract

Significance Atmospheric environmental parameters directly affect the earth's ecological environment and climate changes, and even human life and health. For example, aerosols, clouds, and greenhouse gases affect the radiation balance between the sun and the earth through sunlight absorption and scattering, which is an important cause of atmospheric environmental pollution and frequent extreme weather. Additionally, the atmosphere is an aerospace operation area, and environmental parameters such as atmospheric temperature, pressure, density, and atmospheric wind field exert a decisive influence on the design and performance indicators of the equipment. Therefore, the detection of global atmospheric environmental parameters has caught much attention from scholars all over the world.

Satellite remote sensing is an important technical means to obtain global atmospheric environment parameters, and can be divided into active and passive detections. Active detection of its radiation source is to emit different forms of electromagnetic waves to the target. Meanwhile, it does not depend on sunlight and can work day and night. Passive detection of its non-radiation source needs to rely on the reflection of the target object or the electromagnetic wave of the natural radiation source (such as the sun). Compared with the active spaceborne detection technology, the passive detection payloads have a long history, mature technology, and diversified types of remote sensing instruments and detection targets, but there are some problems such as reliance on sunlight, detection time, and regional limitations. The active spaceborne detection technology represented by lidar makes up for these shortcomings, and the active and passive spaceborne remote sensing atmospheric detection technologies are developed jointly to provide strong technical support for the detection of global atmospheric environmental parameters.

Currently, atmospheric environment detection of satellite remote sensing has made great contributions to the detection of clouds, aerosols, atmospheric wind fields, greenhouse gases, temperature, pressure, density, and other parameters, and solved the problems of air pollution, climate changes, and national defense applications. We introduce the development history of spaceborne lidar and focus on the comparative analysis of the advantages and disadvantages of

active and passive spaceborne remote sensing payloads for detecting major atmospheric environmental parameters. Finally, the future development trend of atmospheric environmental parameter detection technology in spaceborne lidar and passive remote sensing is summarized.

Progress Since the launch of LITE in the United States, domestic extraterrestrial lidars have developed rapidly for nearly 30 years, and the atmospheric parameters that can be detected mainly include clouds, aerosols, greenhouse gases, and atmospheric wind fields. Although LITE has a short working time, it lays a good foundation for spaceborne lidar atmospheric detection with milestone significance. The ice, cloud, and land elevation satellite (ICESat) carries the geoscience laser altimeter system (GLAS) and is the world's first earth observation laser altimeter satellite. As a follow-up mission to ICESat, the ICESAT-2 satellite is launched by the national aeronautics and space administration of America (NASA) in September 2018, and is equipped with the advanced topographic laser altimeter system (ATLAS) (Fig. 1). Developed by NASA in collaboration with the French National Space Research Center (CNES), CALIOP is a major breakthrough in the development of spaceborne lidar technology and has been in orbit for 17 years now, far exceeding the expected design. Scientific data are provided for such scientific issues as aerosol-cloud-precipitation interactions, global dust distribution, transport and pollution, and studies on weather and climate changes (Fig. 2). As the only lidar system aboard the space station to date, CATS employs photon counting methods to obtain vertical cloud and aerosol distribution characteristics (Fig. 3). To obtain information about the three-dimensional wind field of the global atmosphere, the European Space Agency (ESA) launched the ADM-Aeolus satellite on August 22, 2018, carrying the Atmospheric Laser Doppler Instrument (ALADIN). It is the first Doppler wind measurement lidar to acquire the global atmospheric wind field. This indicates the high precision and strong real-time wind measurement capability of spaceborne lidar and has made great contributions to improving the weather and climate forecasting accuracy, optimizing atmospheric models, and advancing atmospheric dynamics research (Fig. 4). Domestic spaceborne lidar started late. On April 16, 2022, China launched the aerosol and carbon dioxide detection lidar (ACDL) on the atmospheric environmental monitoring satellite (DQ-1). Based on path integral laser differential absorption (IPDA) and high spectral resolution lidar (HSRL) technologies, atmospheric environmental parameters can be obtained, such as global cloud, aerosol vertical profile distribution, and CO₂ column line concentration in full time and with high accuracy. It is also the only on-orbit spaceborne lidar actively detecting greenhouse gases globally (Fig. 5). Spaceborne lidars such as ASCENDS, A-Scope, and MERLIN are also based on IPDA. The platforms and main technical parameters of these spaceborne lidar are shown in Table 1.

There are many kinds of passive spaceborne remote sensing for cloud, aerosol, greenhouse gas, and atmospheric wind field loads, and the inversion algorithms are diverse and mature. In 1960, the United States launched the first meteorological satellite TIROS-1 to open a new era of satellite cloud remote sensing observation. The representative of China is the Fengyun meteorological satellite series. The moderate resolution imaging spectroradiometers (MODIS) in the United States launched on the Terra and Aqua satellites and the Himawari series in Japan show good results in cloud remote sensing. There are many kinds of spaceborne passive remote sensing of aerosols and can be roughly divided into the following categories: multi-spectral remote sensing instruments, polarization remote sensing instruments, and multi-angle remote sensing instruments, such as AVHRR, DPC, MODIS, and MISR. In the passive satellite remote sensing of greenhouse gases, the most representative ones are Japan's GOSAT series, the United States' OCO series, and China's GF-5. The atmospheric wind field of passive spaceborne remote sensing mainly takes cloud, water vapor, and atmospheric composition as detection targets for inversion, including MERSI-II, AGRI, DPC, MODIS, and AHI.

Conclusions and Prospects Satellite remote sensing is an effective means to obtain global atmospheric parameters and provide scientific data support for global environmental and climate changes. The development of passive spaceborne remote sensing starts earlier with more mature technology and more abundant atmospheric environment parameters that can be detected. However, passive remote sensing has inevitable disadvantages, such as low accuracy, incomplete coverage of high latitude areas, and lack of night detection data. As a typical active remote sensing equipment, lidar features high precision and high spatio-temporal resolution, which can make up for the shortcomings of passive remote sensing. At present, ground-based and airborne atmospheric lidar detection has been quite mature, and spaceborne lidar remote sensing detection is the future development trend, which has developed for nearly 30 years since the launch of LITE. The atmospheric parameters that can be detected mainly include clouds, aerosols, greenhouse gases, and atmospheric wind fields. Through comparative analysis, the advantages and disadvantages of active and passive spaceborne remote sensing detection technology of atmospheric environmental parameters are revealed. According to different application scenarios and needs, the appropriate detection methods are chosen.

Key words spaceborne lidar; active and passive remote sensing; optical payload; atmospheric environmental parameters; atmospheric detection